Meteorol. Z. (Contrib. Atm. Sci.), Vol. 34 (2025), 125–148
Published online June 12, 2025

Open Access
Urban Meteorology

Characterization of potential temperature hotspots during urban heat island episodes examined by large eddy simulation and land use regression for the city of Augsburg

Annette Straub[1,*], Christoph Beck[1], David Jean du Preez[2], Christoph Knote[2], Christopher Claus Holst[3], Andreas Philipp[1]

[1] Institute of Geography, University of Augsburg, Augsburg, Germany, Alter Postweg 118, 86159 Augsburg
[2] Model-based Environmental Exposure Science, Faculty of Medicine, University of Augsburg, Augsburg, Germany, Werner-von-Siemens-Straße 6, 86159 Augsburg
[3] Institute of Meteorology and Climate Research – Atmospheric Environmental Research (IMK-IFU), Karlsruhe Institute of Technology (KIT), Garmisch-Partenkirchen, Germany, Kreuzeckbahnstraße 19, 82467 Garmisch-Partenkirchen
* Corresponding author: annette.straub@geo.uni-augsburg.de

With 10 figures and 5 tables

Abstract: This study investigates the spatio-temporal distribution of potential temperature (theta) hot- and coldspots in an urban environment for one day during a summerly heat wave, as reflected by a large eddy simulation (LES) model as well as reproduced by a multiple linear regression (MLR) model based on an observation network. The spatial variation of static surface characteristics only partly explains the observed patterns for both approaches. The question of which additional factors, mainly those related to atmospheric circulation, are essential for the development of theta hot- and coldspots is addressed. For this purpose, real case simulations with the LES model PALM-4U were conducted for the city of Augsburg, Southern Germany. Hot- and coldspots were detected in the modelled theta fields with the G_i* statistic. The theta and G_i* patterns were compared to the results of the MLR model, using only static surface characteristics for the referring daytime, season and weather type as predictors. For some times of the day, the patterns from the two approaches show good agreement, but there are considerable differences for other situations, although the weather type does not change over the studied period. In a next step, the detected hotspots are classified into expected and unexpected hotspots according to their surface characteristics, and differences in the meteorological variables for both groups are investigated. A similar procedure is applied to areas apart from hotspots, which could be expected to be hotspots, and those which are not expected to be one. The results indicate that even in summerly anticyclonic conditions with low wind speeds, horizontal circulation and vertical mixing play a significant role in manifesting urban theta patterns. It is concluded that more than a single simulation may be required to represent typical urban temperature patterns during heat waves since they cannot reflect the critical influence of varying circulation dynamics at different synoptic conditions. This should be considered in urban planning.

Keywords: urban temperature; hotspots; PALM-4U; multiple linear regression; G_i* statistic; Augsburg; urban climate

1 Introduction

The fact that the climatic conditions in urban areas are altered compared to their rural surroundings (e.g., Oke 1982) is well documented. The influence on temperature, especially the formation of an urban heat island (UHI), has been investigated profoundly (e.g., Arnfield 2003; Kuttler & Weber 2023). For large cities the formation of urban heat island or urban dome circulations with larger vertical extent has been proposed (i.e., Fan et al. 2017). However, there are also pronounced differences in the thermal conditions within cities, which are attributed to spatial heterogeneity of land use and land cover. Factors such as building density, building geometry, degree of sealing, or vegetation density were reported to affect this variance within urban boundaries (e.g., Fenner et al. 2017; Kim & Brown 2021). The resulting complex spatial pattern of warmer and cooler areas can be appropriately termed an "urban heat archipelago" rather than an even heat island (e.g., Kuttler & Weber 2023). In addition to the variables characterizing the surface type, UHI conditions vary depending on weather type (e.g., Morris et al. 2001; Zak et al. 2020). The resulting atmospheric circulation and three-dimensional structure of the atmospheric boundary layer play an important role in the development of

DOI: 10.1127/metz/1252
Gebrüder Borntraeger Science Publishers, Stuttgart, www.borntraeger-cramer.com

intra-urban temperature differences (e.g., Scherer et al. 2019; Masson et al. 2020). For several cities, measurements and statistical approaches have shown that pronounced UHI conditions occur especially under synoptic situations with low wind speeds and low cloud cover in summer, e.g. for the city of Augsburg, Southern Germany (Beck et al. 2018; Straub et al. 2019; Wild et al. 2022). However, even under such conditions, land surface characteristics cannot fully explain the spatial temperature distribution in an urban area. This can be concluded from the results of statistical models for Augsburg with explained variances of up to 80 % (Straub et al. 2019) and is confirmed by other statistical studies relating land surface variables to temperature, which reach maximum explained variances of up to, e.g., 80 % (Burger et al. 2021), 87 % (Hsu et al. 2020), or 92 % (Alcoforado & Andrade 2006) in the best cases. In order to address the remaining unexplained variance, this study investigates additional, especially circulation-induced variables that might contribute to the development of urban temperature patterns on the micro- to local scale.

Although under future climate change conditions, UHI intensities are not expected to necessarily rise (Hamdi et al. 2020; Masson et al. 2020), more frequent heat waves as well as higher maximum temperatures are projected in cities in Central Europe (Masson et al. 2020) and, thus, health burden by high temperatures is expected to increase (Wouters et al. 2017). For the city of Augsburg, Merkenschlager et al. (2023) found an increase in the number, duration, and spatial extent of summerly heat events under RCP4.5 conditions. As such events pose a serious threat to human health (e.g., Kovats & Hajat 2008; Gasparrini & Armstrong 2011), heat mitigation by e.g. greening, shading, additional water bodies or use of reflective materials (e.g., Lai et al. 2019; Kuttler & Weber 2023) is essential in cities. For urban planners, detailed information on spatio-temporal patterns of temperatures and overheating in individual urban areas is necessary to efficiently implement such heat mitigation measures (Vieira Zezzo et al. 2023).

If spatial temperature data is available, hotspot analysis is a suitable method for detecting the warmest and coolest areas within a study region, and it has been applied in several urban climate studies. Such hotspots and coldspots can be defined in different ways, e.g., by thresholds based on the standard deviation (e.g., Steigerwald et al. 2022; García & Díaz 2023) or by applying the Getis-Ord G_i* statistic after Ord & Getis (1995) and Getis & Ord (1996). The latter has been successfully applied to land surface temperatures from satellite data and, in some cases, on air temperature data from dense urban measurement networks, e.g., for Florence metropolitan area (Guerri et al. 2021), Karaj (Mokhtari et al. 2022) or Shenzhen (Cao et al. 2021) or in a modified version for the city of Karlsruhe (Bruns & Simko 2017). Spatially continuous data are also available from statistical and numerical models.

This study applies the microscale model PALM-4U (Parallelized Large-Eddy Simulation Model for Atmospheric and Oceanic Flows – for Urban Application) in the urban area of Augsburg for a summerly heat episode with anticyclonic conditions. PALM-4U is an LES model that can be applied to large domains in urban areas (Maronga et al. 2020). It has been utilized and evaluated successfully for simulations of the urban boundary layer in various studies, focusing on meteorological variables and air chemistry (Resler et al. 2021), heat exposure (Geletič et al. 2021; Anders et al. 2023), or aerosols (e.g., Karttunen et al. 2020). Additionally, a multiple linear regression (MLR) model for air temperature is applied. An evaluation of PALM-4U and the MLR model against observations, including an investigation of the influence of the mesoscale input data on the results of PALM-4U, is carried out first. Based on validated model simulations, the locations of potential temperature (theta) hot- and coldspots during the selected period are analysed based on the G_i* statistic in a second step. Theta fields and the distribution of hot- and coldspots in both model approaches are compared. Finally, the factors leading to the development of hotspots in unexpected locations, as well as the absence of hotspots in places where a hotspot would be expected due to the surface characteristics, are examined based on the PALM-4U simulation applying statistical methods. It is important to note that these analyses do not investigate any human-biometeorological indices and do not aim at assessing heat stress. Instead, the analysis is applied to potential temperature (theta), i.e. air temperature that would be measured, if all observation points would show the same air pressure, because this is the direct output of the PALM-4U model and can be interpreted without making further assumptions. Therefore, the study does not reflect all factors for thermal health burden but examines one major aspect of it. The term "hotspot" as used in this study therefore refers to a peak in the spatial theta field, rather than a place with thermal heat stress for humans.

2 Material and methods

2.1 Study area

The study area (Fig. 1) comprises a part of the medium-sized city of Augsburg (48.37 °N; 10.90 °E) in the southwestern part of Bavaria, Southern Germany. In December 2019 the city had 296,582 inhabitants and covered an area of 146.87 km² (Stadt Augsburg 2021). Augsburg belongs to the type Cfb of the Köppen-Geiger climate classification (warm temperate climate) as shown by Kottek et al. (2006). It has an annual mean air temperature (T_{air}) of 8.5 °C and humid conditions throughout the year with a mean annual precipitation sum of 768 mm (Beck et al. 2018). Climatic influence on the meso- and local scale can be expected from a chain of forested hills to the west of the city (maximum

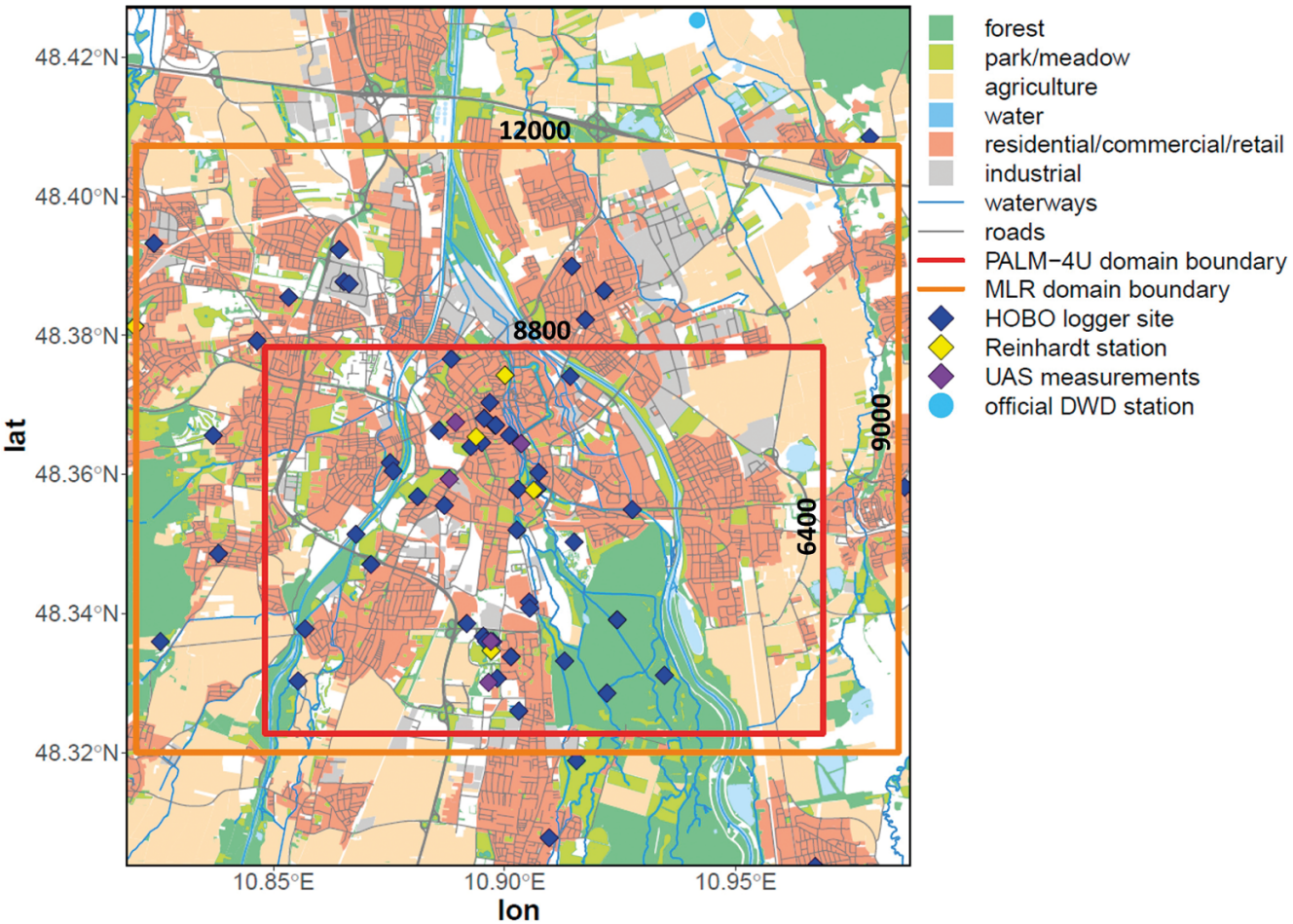

Fig. 1. Location, extent (black numbers at the domain boarders given in meter) and land-use information for the model domain for the PALM-4U simulations (red rectangle) in Augsburg as well as the domain for the MLR model (orange rectangle). Locations of the measurement sites of a stationary network, the flights with unmanned aerial systems (UAS) as well as the official DWD measurement site are included, too. Reinhardt automatic weather stations (AWS) from north to south with height above ground given in brackets: St. Stephan (4.3 m), Königsplatz (8 m), Rotes Tor (9.6 m), University roof (20 m). Height above ground of the HOBO loggers (THL): 1.5 m–2.3 m.

elevation approximately 60 m above the lowest level of the city area), which is however not part of the study area. The two rivers Wertach and Lech and their valleys traverse the area from the south and confluence in the north of the city. Between the rivers quarternary terraces elevate approximately 15 m above the valleys. A large, forested area in the southeast of the city along the Lech river is located in the direct neighbourhood of the built-up area (Fig. 1). The highest building densities belonging to the local climate zone (LCZ, after Stewart & Oke 2012) “compact mid-rise” can be found in the centre, but most of the area of Augsburg is covered by the LCZ “open mid-rise”. In the surroundings of the city, the LCZ “low plants” can be found frequently, and the large, forested area in the southeast of the city is covered by the LCZs “dense trees” and “scattered trees” (Beck et al. 2018).

2.2 Meteorological observation data

Different meteorological measurements are available for the model evaluation. Four automatic weather stations (type MWS9/10, manufacturer: Reinhardt, hereafter referred to as AWS) are deployed in the study area (Fig. 1, yellow rhombs). They record air temperature, relative humidity, horizontal wind speed, wind direction, and various other variables at heights between 4.3 m and 20 m above ground as five-minute mean values. A measurement network of 83 HOBO pro v2 loggers (manufacturer: Onset, hereafter referred to as temperature and humidity logger, THL) for air temperature and relative humidity is installed in Augsburg, 32 of which are distributed over the PALM-4U domain (Fig. 1, blue rhombs). The network is operated jointly by German Research Center for Environmental Health in Munich (Helmholtz Zentrum München) and the University of Augsburg. The first sites

were established in December 2012 (Beck et al. 2018). Their locations represent various microclimatic environments and different local climate zones (LCZ) according to the concept by Stewart & Oke (2012). The data are recorded at heights between 1.5 m and 2.3 m with a temporal resolution of four minutes (instant values) and various quality checks are conducted (Beck et al. 2018). They were utilized for the PALM-4U evaluation and for fitting the MLR models. For the PALM-4U evaluation, they were aggregated to 20 minutes mean values and the mean value was attributed to the last time step in the interval.

Besides, vertical profiles of air temperature and relative humidity were recorded by measurement flights with fixed-wing UAS (unmanned aerial systems) and a hexacopter (M600 from DJI) equipped with SHT75 and SHT85 sensors (manufacturer: Sensirion). For the heat wave episode (25.06.2019 12:00 UTC to 27.06.2019 09:00 UTC, cf. section 2.3), one flight at 7:00 CEST is available in the southern part of the PALM-4U domain. For the reference period (04.06.2019 12:00 UTC to 06.06.2019 06:00 UTC, cf. section 2.3), hourly flights at three different sites in the city were performed between 05.06.2019 05:00 UTC and 06.06.2019 05:00 UTC. These include two inner-city sites and one outside the city centre (Fig. 1). Vertical profiles of wind speed were calculated based on the flight parameters, following Mayer et al. (2012). These measured profiles were compared with the corresponding PALM-4U output to evaluate the model.

Furthermore, hourly measurements from the official station of the German Meteorological Service (DWD, Deutscher Wetterdienst) (DWD Climate Data Center 2024a) were utilized to select the periods modelled with PALM-4U. They also served as a rural temperature reference in the MLR models (see section 2.4). For the evaluation of PALM-4U, all measured T_{air} values were converted into theta, and relative humidity was converted into mixing ratio to match the prognostic variables in PALM-4U. This conversion utilized air pressure measurements from the DWD station (DWD Climate Data Center 2024b). The maximum uncertainty in the theta field resulting from the use of this pressure for the whole study domain despite small elevation differences has been determined not to exceed 0.37 K.

2.3 PALM-4U simulations

Two different periods were selected for the PALM-4U model runs: i) a heat wave episode, which was simulated twice with different synoptic forcings, and ii) a period with average temperature conditions.

The first period from 25.06.2019 12:00 UTC to 27.06.2019 09:00 UTC is part of a heat wave with maximum T_{air} of 34.3 °C in the afternoon at the station Augsburg Mühlhausen from DWD in the rural surroundings of the city. Because of these high T_{air} and the two preceding days also reaching T_{air} above 30 °C, this period can be considered a heat wave situation. The DWD defines a hot day as a day with maximum temperatures of at least 30 °C, a definition also applied by e.g. Tomczyk (2018). Heat wave definitions are not uniform but usually include a minimum duration of e.g. three days exceeding a temperature threshold (as e.g. in Mücke & Litvinovitch 2020). In addition, the atmospheric circulation on that day is characterized by anticyclonic conditions and weak synoptic forcing with maximum wind speeds of 2.9 m/s and an average wind speed of 1.3 m/s at 9 m above the ground (which is the height of the wind sensor at the DWD station). The mesoscale dynamic forcing for this run came from the COSMO-D2 model from DWD and was generated with the INIFOR tool (Kadasch et al. 2021). The mesoscale input provides PALM-4U with initial atmospheric and soil conditions. It also provides time-variant hourly input of atmospheric variables as cross sections along the PALM-4U lateral boundaries and top (Kadasch et al. 2021). As the modelled episodes are not entirely free of clouds, the effect of clouds on incoming shortwave radiation was taken into account utilizing measurements of global radiation from the AWS at the University roof. Cloud cover measurements from a ceilometer at the University roof were used to estimate the incoming longwave radiation after Unsworth & Monteith (1975) and Dilley & O'Brien (1998). This simulation was utilized to find and analyse theta hot- and coldspots in Augsburg. Another run was conducted for this heat wave episode (25.06.2019 12:00 UTC to 27.06.2019 00:00 UTC) with mesoscale forcing from a WRF-Chem run instead of the COSMO-D2 run (for the WRF-Chem setup see Knote et al. 2015). The latter dynamic driver was created using a tool developed at the Chair for Model-based Environmental Exposure Science, University of Augsburg, based on the WRF4PALM tool after Lin et al. (2021). This run was utilized to estimate the influence of the dynamic input on the PALM-4U results.

The second period, 04.06.2019 12:00 UTC to 06.06.2019 06:00 UTC, is used as a reference situation and is utilized in this study for the model evaluation only. This summer day is characterized by more moderate T_{air} of up to 27.9 °C and higher wind speeds of up to 5.3 m/s, with 2.7 m/s on average at 9 m above the ground and consequently more vertical mixing. On that day, a measurement campaign took place in Augsburg. Vertical T_{air} and relative humidity profiles were measured with unmanned aerial vehicles at three different sites in the city. The flights were carried out hourly and covered the lower part of the urban boundary layer up to 500 m above the ground. This makes the day particularly suitable for model evaluation as it allows us to evaluate the three-dimensional structure of the boundary layer. This run was forced using a dynamic driver generated from the output of the COSMO-D2 model.

All simulations were carried out with the PALM-4U model system, version 21.10-rc1. The model setup comprises a model domain (Fig. 1) with 880 × 640 × 256 grid points and a grid spacing of 10 m. In order to save computational time, the grid is stretched vertically above 2000 m

with a factor of 1.08. The resulting domain height amounts to approximately 4000 m and, thus, covers the boundary layer completely. The model domain covers a large part of the city of Augsburg, with dense buildings, a high proportion of sealed surfaces in the inner-city, and various smaller parks. The domain also covers the two rivers and the large, forested area in the southeast (Fig. 1). The altitude differences in the PALM-4U domain amount to approximately 35 m. The static driver (time-invariable surface and land cover characteristics) includes the elevation from a digital terrain model provided by the Bavarian Agency for Digitisation, High-Speed Internet and Surveying (LDBV). Building locations, height, and type come from a LoD2 building model from LDBV. Open Street Map was used to derive vegetation type, pavement type, water type, and street type, according to Heldens et al. (2020). Vegetation heights of large, contiguous tree populations were derived from lidar data from LDBV to create three-dimensional tree information for the model domain. Due to a lack of data, the soil type was set to a uniform value of "medium-fine" for the whole domain. The temporal resolution of the PALM-4U output was set to five minutes and aggregated to 20 minutes mean values analogous to the THL data for the comparison with the measurements from this network. PALM-4U's wall and soil surface spin-up mechanism (Maronga et al. 2020) was applied for the 30 hours advancing the actual beginning of the simulation period in both runs. All simulations were carried out on three compute nodes with AMD EPYC processors, each with 128 CPUs.

2.4 MLR models for the spatial distribution of potential temperature

Continuous spatial fields of urban heat island intensity were modelled with multiple linear regression (MLR) for different times of day, seasons, and weather situations (Table 1) based on the observation network data (THL). The MLR models are based on previous work by Straub et al. (2019), but some adaptations were made. Predictors include the elevation, the percentage of coverage of different land cover characteristics (forest, buildings, water, park, roads, railway, meadow, farmland, built-up, low vegetation) in different radii (500 m, 250 m, 100 m, 50 m, 25 m) as well as the sky view factor, the distance to the city centre and the distance to natural surfaces with potential cooling effect. The sky view factor (SVF) was found to be an essential predictor for T_{air} in Augsburg but could not be included in the former version of the MLR models because of missing data. In order to improve the results, the SVF was estimated for the whole study area by applying the geographic information system GRASS Gis (Geographic Resources Analysis Support System) plugin r.skyview on a digital surface model with a horizontal resolution of 1 m. Thus, buildings and trees are included in the area-wide, high-resolution calculation of the SVF. A stepwise approach was used for the final predictor selection (cf. Table 4). The domain was extended to cover an area of 12 km × 10 km and includes the built-up area of Augsburg, some of its surroundings, and the whole PALM-4U domain (Fig. 1). Besides, a distinction of five instead of three times of day was implemented. This allows for a more subtle differentiation and helps to cover the characteristic processes in the daily cycle of the boundary layer evolution. The time intervals were selected based on the daily cycle of the height of the planetary boundary layer observed with a ceilometer at the roof station at the University of Augsburg for the simulated day, the evolution of turbulence intensity in the PALM-4U simulation, and theoretical considerations about the daily cycle of the planetary boundary layer from Stull (1988). The five different time intervals are given in UTC and comprise morning, noon, evening, and night, where night is divided into first and second half. Morning is defined as the time from 8:00 to 10:00 when turbulence intensity increases, the boundary layer grows, and a mixed layer develops. The time directly after sunrise was excluded from the interval because PALM-4U's exact times of the onset of turbulence development can differ from reality because PALM-4U cannot resolve initial sub grid scale turbulence. Noon covers the

Table 1. Overview of situations differentiated by season, time of day and weather situation based on cloud cover ("cc") [octas] and wind speed ("ws") [m/s], which are covered by the MLR models.

Seasons:	**MAM**	**JJA**	**SON**	**DJF**		
	March–May	June–August	September–November	December–February		
times of day:	**morning**	**noon**	**evening**	**1st half of the night**	**2nd half of the night**	
	8 a.m.–10 a.m.	12 a.m.–2 p.m.	5 p.m.–7 p.m.	10 p.m.–11 p.m.	2 a.m.–4 a.m.	
weather situations:	**clear & calm**	**clear & intermediate wind speed**	**clear & windy**	**cloudy & calm**	**cloudy & intermediate wind speed**	**cloudy & calm**
	cc: 0–3	cc: 0–3	cc: 0–3	cc: 4–8	cc: 4–8	cc: 4–8
	ws: 0–2	ws: 2–7	ws: >7	ws: 0–2	ws: 2–7	ws: >7

time from 12:00 to 14:00 when the boundary layer is well mixed and reaches its maximum depth. The interval from 17:00 to 19:00 is included for the evening, which is the time before sunset. Turbulence is already decreasing, and the height of the boundary layer is shrinking. The first half of the night covers 22:00 and 23:00, which represents the time after sunset when maximum values of the urban heat island intensity can be expected (Oke 1982); some turbulence remains, but a stable boundary layer is beginning to develop. The second half of the night includes the time from 2:00 to 4:00, the time before sunrise with the general daily minimum of T_{air}. Turbulence intensity and the boundary layer height reach their minimum, and a stable stratification is established. The resulting time intervals, thus, are distinctly different from one another, relatively homogenous in themselves and represent characteristic conditions in the daily evolution of the boundary layer. Besides considering SVF and the different daytime intervals outlined above, another improvement of the MLR models is the utilization of a more extended time series at all measurement stations (six years of additional data, resulting in ten years) and the inclusion of newly established stations of the THL network. Three new forest sites should especially be highlighted because forested areas were underrepresented in the former version of the MLR model.

Finally, the MLR models for summer and calm and clear conditions and the hourly T_{air} measurements from the DWD station were applied to estimate the T_{air} fields for the heat wave situation. In order to compare these MLR model results with the PALM-4U results, the T_{air} fields were converted to theta using the same methodology as for the conversion of the measured data (see section 2.2). This was done for all time intervals: the second half of the night before the heat day (26.6.), morning, noon, evening, the first half of the night on the heat day (26.6.), and the second half of the night after the heat day (27.6.). As the whole period belongs to the same weather category (calm and clear), the MLR models for the second half of the night on 26.6. and 27.6. are identical.

The resulting theta fields were compared with theta fields from PALM-4U averaged in each time interval modelled with the MLR. For the comparison the fields from both models were z-standardised by subtracting the mean value and dividing by the standard deviation to take the bias of theta in PALM-4U into account (cf. section 3.1.1). The maps of z-standardized theta values were compared (cf. Fig. 5), and the correlation between the theta maps of the MLR model and the PALM-4U model was examined by applying the modified t-test after Dutilleul et al. (1993), which uses a reduced number of degrees of freedom to account for the spatial autocorrelation of the fields, respectively.

2.5 Detection and analysis of hot- and coldspots

The R package "spdep" was applied to calculate the Getis-Ord G_i^* statistic (e.g., Ord & Getis 1995) for the detection of hot- and coldspots in the theta fields at 2 m above the ground from PALM-4U and the MLR models. This statistic takes a region (in this case a grid point) and the neighbouring areas (i.e., surrounding grid points within relatively large radii) around the central grid point into account to look for significantly hot and cool areas compared to the mean value of the field (Getis & Ord 1996). So, in this study, hotspots and coldspots are defined as clusters of grid points with high or low theta, respectively, and will be referred to as hot- and coldspots hereafter. The resulting values of G_i^* are z-scores, which can be assumed to follow a standard normal distribution even if the distribution of the original data is skewed assuming the number of included neighbours is sufficiently large (Getis & Ord 1996). In this case, the directly neighbouring grid points were included. The z-scores show if a grid point belongs to a hot- or coldspot and also contain information on the significance of the detected hot- and coldspots (Ord & Getis 1995; Getis & Ord 1996; Bivand & Wong 2018).

For the five daytime intervals defined in section 2.4, values of G_i^* were evaluated for the time-averaged theta fields from the PALM-4U heat wave simulation results. To reduce the influence of lateral boundary effects, an area of 500 m at each model boundary of the PALM-4U domain was excluded from this analysis. Equivalently, G_i^* was calculated for the theta fields from the MLR for the five time intervals. The resulting G_i^* maps from PALM-4U and MLR were compared.

In the next step, the significant hotspots ($\alpha < 0.05$) detected in the PALM-4U theta field, as well as the areas apart from these hotspots (insignificant G_i^* value or significant coldspots, also from PALM-4U), were characterized by different land cover characteristics from the static PALM-4U input on the one hand and time dependent meteorological variables from the PALM-4U output on the other hand. The former include mean and maximum building height, building volume, percentage of sealed area, sky view factor, percentage of vegetated area, and albedo. The latter include horizontal wind speed at the lowest grid point, in the canopy layer and above the canopy layer as well as the absolute vertical velocity, the turbulence intensity, theta, mixing ratio, shortwave incoming radiation, and the various heat fluxes within the canopy layer. The vertical shear of horizontal wind speed and the lapse rate of theta, both within the boundary layer, were calculated from the PALM-4U output and used as additional measures for turbulence and atmospheric stability, respectively. Here, the boundary layer height was estimated by visual assessment of vertical profiles for each time interval as the height where turbulence intensity decreases rapidly.

Then, the hotspots detected in the PALM-4U output were categorized into expected and unexpected hotspots based on their respective land cover characteristics. Unexpected hotspots were defined as grid points that are outliers in at least one of the surface variables. Outliers were defined as values lower or higher than the 1.5-fold interquartile range from the first or third quartile, respectively, depending on

the variable. For example, an unexpected hotspot could be defined by unusually low building cover or unusually high vegetation cover. The insignificant areas and coldspots were categorized into those where a hotspot could be expected due to the surface cover and those where no hotspot is expected. This differentiation was based on values higher than the third quartile or lower than the first quartile, again depending on the variable. The results for the different variables were combined in the following way: An unexpectedly missing hotspot is defined as a spot with large building cover or volume and low vegetation cover, large percentage of sealed area and low vegetation cover or low albedo. For both the expected and unexpected hotspots on the one hand and the expectedly and unexpectedly missing hotspots on the other hand, a Mann-Whitney U-test was performed for the meteorological variables to find significant differences ($\alpha < 0.05$) between the respective samples.

Finally, backward trajectories for the expected, unexpected and unexpectedly missing hotspots were calculated using the averaged three-dimensional wind field for each of the five time intervals defined in section 2.4. Trajectories were calculated for five minutes, but trajectories reaching the domain boundary within five minutes travel duration were excluded in order to keep comparability and to avoid artefacts arising from discontinuities at the PALM-4U model domain boundary. The positions of the virtual parcels were calculated every three seconds. In some rare cases where the trajectories get stuck in building corners as a dead end, resulting from the averaging of the wind field, the particles were lifted above the building. For each time step along the trajectories the theta, turbulent kinetic energy, speed and height above ground level was determined and aggregated to average values for the whole trajectory over the five minutes travel time. This allows to estimate the impacts of circulation not only directly at the location of the hotspots but also by the history of the advected air masses along their path before reaching the hotspots. The trajectories were analysed using a Kruskal-Wallis test for the selected variables aggregated for the travel path to detect significant differences between the three groups.

3 Results

3.1 Model evaluation

3.1.1 PALM-4U evaluation

For the PALM-4U evaluation, the first twelve hours of the simulations were omitted to exclude unphysical effects possibly remaining after the wall and soil surface spin-up, as it is done, e.g., by Vogel et al. (2022). Results for comparing time series of theta and mixing ratio values derived from THL and AWS measurements (section 2.2) with the PALM-4U output generally show lower values of theta and mixing ratio in the model (Table 2). These deviations result primarily from the mesoscale forcing using COSMO-D2 output (cf. Fig. 4). Differences in the mean bias at THL stations compared to AWS could be due to the different temporal resolution of the time series (20 minutes vs. 5 minutes). Besides, more minor deviations can be observed in evaluating vertical profiles compared to those for ground-based stations. This could result from higher model uncertainties at near-surface grid points. The absolute values of the mean bias for theta and mixing ratio are smaller for the reference run compared to

Table 2. Mean values of bias and explained variance (R^2) for potential temperature (theta, K), mixing ratio (q, g/kg) and wind speed (ws, m/s) in the model domain of two real case PALM-4U runs in Augsburg (run for the heat wave forced with COSMO-D2 "tb03", run for the reference situation "tn01"), differentiated by measurement device/type of measurement. Numbers in square brackets in the first column give the number of available stations. The comparison for THL and AWS is based on time series of measurements and the corresponding time series of model grid points surrounding the measurement station (mean of 3 × 3 grid points around the coordinate of the station). The temporal resolution of the compared time series is 20 minutes for the THL and 5 minutes for the AWS. The comparison for UAS flights is based on vertical profiles, hourly or single ones depending on the measurement site, and the corresponding profile of model grid points. IGUA = site at the institute of geography, University of Augsburg.

	theta (K)		q (g/kg)		ws (m/s)	
	tb03	tn01	tb03	tn01	tb03	tn01
Mean bias THL stations [tb03: 32; tn01: 29]	−1.5	−2.2	−0.7	−0.3	–	–
Mean bias AWS [4]	−2.5	−2.2	−1.3	−0.6	−1.7	−1.5
Mean bias UAS flights inner-city [2], copter	–	−0.7	–	0.5	–	3.6
Mean bias UAS flights at site IGUA, copter	–	1.2	–	0.5	–	1.2
bias UAS flight at university, 7:00 CEST [1 flight]	−2.3	−3.1	1.0	−0.7	2.4	5.0
Mean R^2 THL stations [tb03: 32; tn01: 29]	96.2 %	93.7 %	38.1 %	34.7 %	–	–
Mean R^2 AWS [4]	88.5 %	89.5 %	25.2 %	27.3 %	10.2 %	13.4 %
Mean R^2 UAS flights inner-city [2]	–	57.8 %	–	46.3 %	–	60.8 %
Mean R^2 UAS flights IGUA	–	41.1 %	–	53.1 %	–	38.6 %
R^2 UAS flight at university, 7:00 CEST	87.0 %	95.7 %	77.7 %	32.7 %	47.2 %	22.9 %

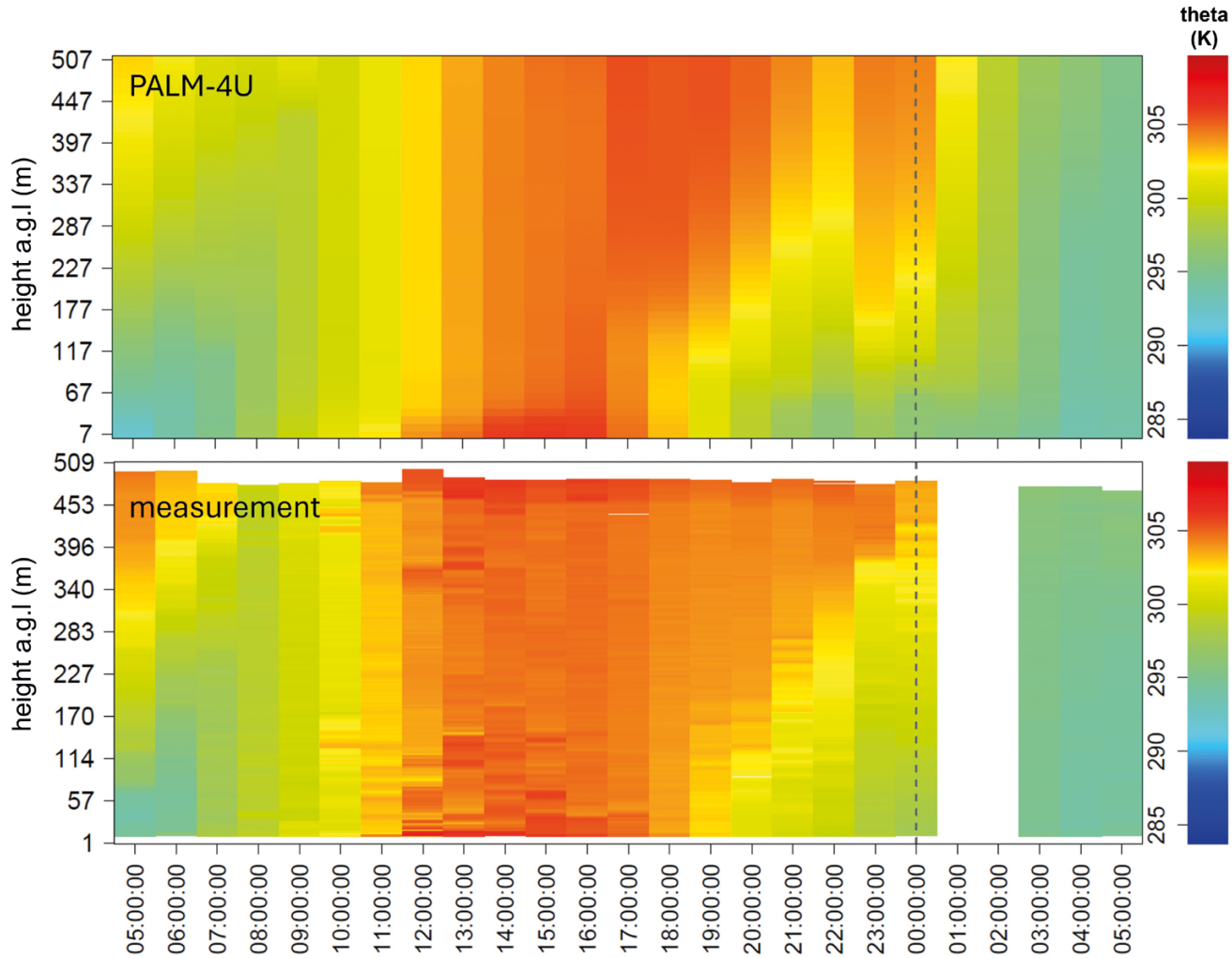

Fig. 2. Time series of vertical profiles of potential temperature for the time period from 05.06.2019 5:00 UTC until 06.06.2019 5:00 UTC (reference run) at the inner-city measurement site “Prinzregentenplatz” in Augsburg. above: PALM-4U, below: measurements with a hexacopter.

the run for the heat day. The values of explained variance are similar for both runs for the comparison of near-surface time series as well as vertical profiles. However, there are differences of R^2 between different meteorological variables and for each variable it varies between different measurement devices. Especially for theta, R^2 has high values for time series and some profiles. Thus, in some situations, the vertical structure of the boundary layer is described well in the model runs. The vertical profiles of the wind speeds show higher values in the PALM-4U runs compared to the measurements, but in the model there is an underestimation of wind speeds near the ground (Table 2).

A time series of vertical profiles of theta for the thermal reference situation at an inner-city site shows an inversion between approximately 100 m and 340 m above ground and a residual layer above for the beginning of the period shown in Fig. 2. This is present in both the measurements and weaker in PALM-4U. In the morning, the heating of the atmosphere from the ground happens parallel in the model and the observations. Temporal deviations may result from the inability of PALM-4U to resolve initial sub grid scale turbulence and, consequently, a slightly delayed development of the planetary boundary layer. The warming results in a neutrally stratified mixed layer at noon and the afternoon with slightly higher theta in the lower 50 m of the boundary layer in the model and the measurements. In the evening, the model starts to cool down earlier and faster than the observations, but from 19:00 UTC, this cooling proceeds synchronously. An exception is a warming in the upper part of the model’s profiles around midnight, which is not observed in the measurements. This comes with a distinctly lower inversion height compared to the measurements. Overall, the plots show a good agreement of the temporal evolution of the lower 500 m of the urban boundary layer for the reference run (Fig. 2).

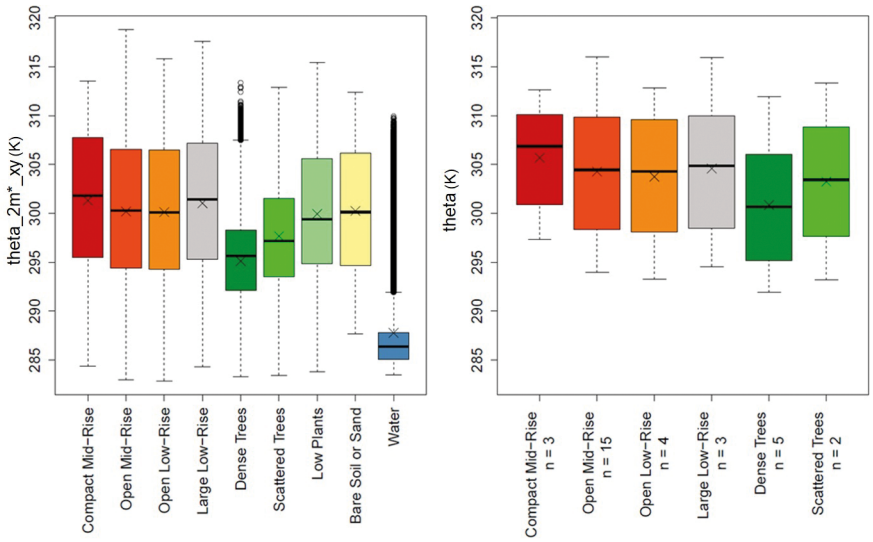

Fig. 3. Boxplots of potential temperature in Augsburg differentiated by LCZ for 26.06.2019. The x indicates the respective mean value. Left: values from PALM-4U at 2 m above ground for the model run for the heat wave episode. Right: values from the measurement network for the same day, numbers on the x-axis give the number of measurement sites per LCZ. Boxplots are defined as follows: the bold line in the boxes indicates the medians of the respective boxes, the lower and upper boundary of the box indicate the 1st and 3rd quartile, respectively, the whiskers indicate the 1.5-fold interquartile range from the boundary of the box, and the dots are outliers.

Fig. 3 shows boxplots and mean values of theta from the PALM-4U domain and the measurement network in different LCZ for the modelled heat day. Inner-city theta variance is represented well by the model. In both cases, all the built-up LCZs are warmer than the vegetated ones. The "compact mid-rise" zone shows the highest theta in the model and the measurements. Regarding the vegetated zones, "dense trees" is colder than "scattered trees" in both cases.

Consequently, despite the lower theta level in the PALM-4U simulations compared with observations, which result mainly from the mesoscale input (see section 3.1.2), the theta variances within the city seem to form a reliable basis for further analyses. No observations are available for the classes "low-plants" and "bare soil or sand," but their modelled theta levels are as expected compared to the other LCZs. As water surface temperatures in PALM-4U are kept at a constant value throughout the simulation, the air and potential temperature at these grid points must be interpreted carefully.

3.1.2 Influence of the mesoscale forcing on PALM-4U results

The PALM-4U theta input for the two simulations of the heat day with different mesoscale forcing is compared in Fig. 4. The differences in the dynamic drivers generated from WRF and COSMO-D2 output, respectively, are visible along with the theta calculated from measurements from the official DWD station. For the first afternoon in the run, WRF generates higher theta than COSMO-D2 and corresponds well with the observations at the DWD station. However, the two mesoscale models show only minor differences for the night and especially for the second day. Both overestimate the nocturnal theta values and underestimate the theta around noon.

The mean theta bias was calculated separately for both days of the runs and the two measurement device types. For this comparison, the simulations' first hour was omitted to exclude spin-up effects remaining after the wall and soil surface spin-up (cf. section 2.3), but include the first afternoon of the simulations, because the largest differences between the two dynamic drivers occur then. Table 3 shows that for the simulation with mesoscale forcing from WRF, the mean theta bias of all measurement stations in the PALM-4U model domain is distinctly smaller on the first day of the run. This is true for the THL and the AWS. The cold bias results mainly from the differences by day and is distinctly smaller during the period without incoming shortwave radiation. On the second day, however, the mean bias of the two runs is very similar. Here, the deviations by day are also larger than at night.

3.1.3 Evaluation of the MLR models

The MLR models show good agreement with the observations from the THL network, especially in the evening and night. The explained variances reach values from 38 % up to 72 % in the fitting procedure and still have values between 16 % and 68 % in the leave-one-out cross-validation. The MSE is small, with some values around or below 0.5 K and up to approximately 1 K. The explained variances are distinctly lower in the morning and noon compared to other times of the day, but the MSE is still relatively low, with

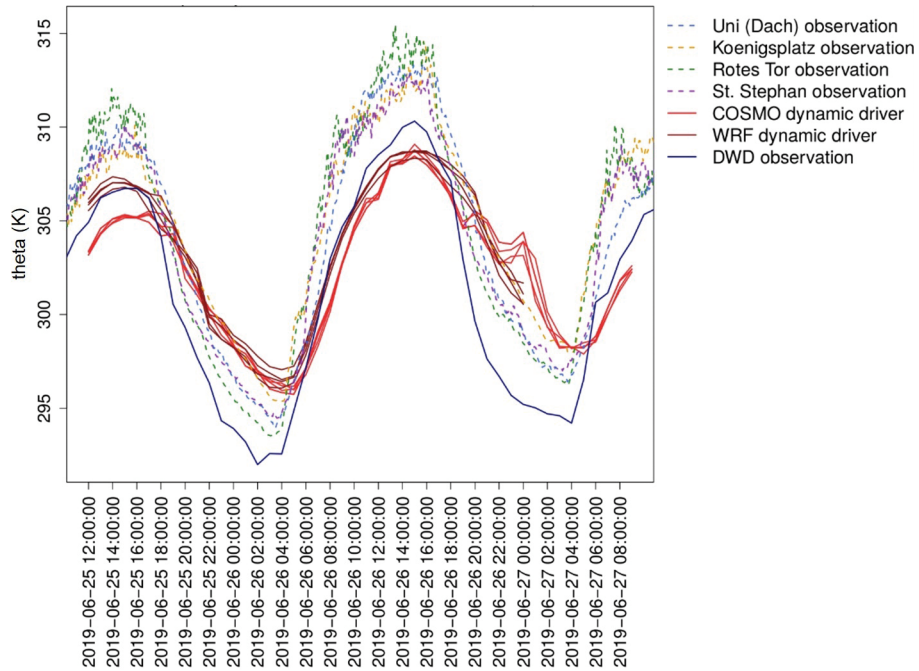

Fig. 4. Time series of near ground values of the potential temperature from the two dynamic drivers (each of the four red and brown lines, respectively, representing the theta value given as mesoscale input from COSMO-D2 and WRF, respectively, along one lateral boundary of the PALM-4U domain) as well as observations from the official DWD station and four inner-city automatic weather stations.

Table 3. Mean bias of the potential temperature in PALM-4U for the two runs with different mesoscale forcing, differentiated by station type, simulated day and time of day.

		forcing with COSMO-D2			forcing with WRF		
		all day	period with incoming shortwave radiation	period without incoming shortwave radiation	all day	period with incoming shortwave radiation	period without incoming shortwave radiation
25.06.2019	THL	−1.7 K	−2.1 K	−1.1 K	−0.8 K	−0.8 K	−0.8 K
	AWS	−2.1 K	−2.6 K	−0.4 K	−1.4 K	−1.3 K	−0.3 K
26.06.2019	THL	−1.5 K	−1.6 K	−1.3 K	−1.4 K	−1.4 K	−1.3 K
	AWS	−3.0 K	−3.6 K	−0.5 K	−2.8 K	−3.2 K	−0.4 K

maximum values of 1 K in the leave-one-out cross-validation (Table 4).

3.2 Comparison of PALM-4U and MLR

The comparison of spatial theta fields from MLR and PALM-4U (sample size: 22528 grid points, degrees of freedom between 12 and 19 depending on time of day) shows good agreement and the correlations between the fields are highly significant ($\alpha = 0.01$) for most time intervals. Correlation coefficients reach up to 0.92 at noon and are also high in the other situations for the run with mesoscale forcing from COSMO-D2. Only in the second half of the first night did the correlation between the models reach intermediate values (Table 5). For the run with mesoscale forcing from WRF, the theta field correlations show comparable values.

Fig. 5 shows z-standardized theta maps from the PALM-4U simulation with dynamic forcing from COSMO-D2 on the right and MLR on the left, including measurements from the THL network for noon (Fig. 5 above) and the first half of the night after the heat day (Fig. 5 below). Although the absolute near-surface theta values from PALM-4U are lower than the measurements (see section 3.1) and aside from showing different levels of detail due to different horizontal resolutions, the maps show similar spatial theta patterns from PALM-4U and MLR for both selected times of the day. At noon, distinctly cool areas are in the forest and along the rivers in both

Table 4. Evaluation of the MLR for different times of day against the THL observations applying R^2 and the mean square error (MSE) for the fitting and leave-one-out cross validation (LOOCV). The last column shows the predictors selected in the models by the stepwise approach (numbers indicate the radius, dc=distance to city centre, svf=sky view factor).

time of day	R^2 (fit)	MSE (fit)	R^2 (LOOCV)	MSE (LOOCV)	final predictors
morning	44 %	0.47 K	21 %	0.72 K	buildings 500 + forest 50 + svf
noon	38 %	0.71 K	16 %	1 K	forest 500 + roads 250 + svf
evening	72 %	0.28 K	68 %	0.31 K	buildings 500 + forest 500 + dc
1st half of the night	65 %	0.85 K	60 %	0.97 K	buildings 500 + roads 500
2nd half of the night	72 %	0.53 K	66 %	0.65 K	buildings 500 + roads 500 + dc

Table 5. Correlation coefficients (r) and p-values for the t-test between the potential temperature fields from MLR and PALM-4U for different time intervals for the simulated heat situation including the 2nd half of the night on 26.06.2019 (night before the actual heat day) until the 2nd half of the night on 27.06.2019 (night after the heat day).

		2nd half of the night (before heat day)	morning	noon	evening	1st half of the night	2nd half of the night (after heat day)
run with COSMO-D2 forcing	r	0.52	0.90	0.92	0.89	0.75	0.72
	p-value	0.03	0	0	0	0	0.002
run with WRF forcing	r	0.64	0.89	0.92	0.91	0.67	–
	p-value	0.007	0	0	0	0.002	–

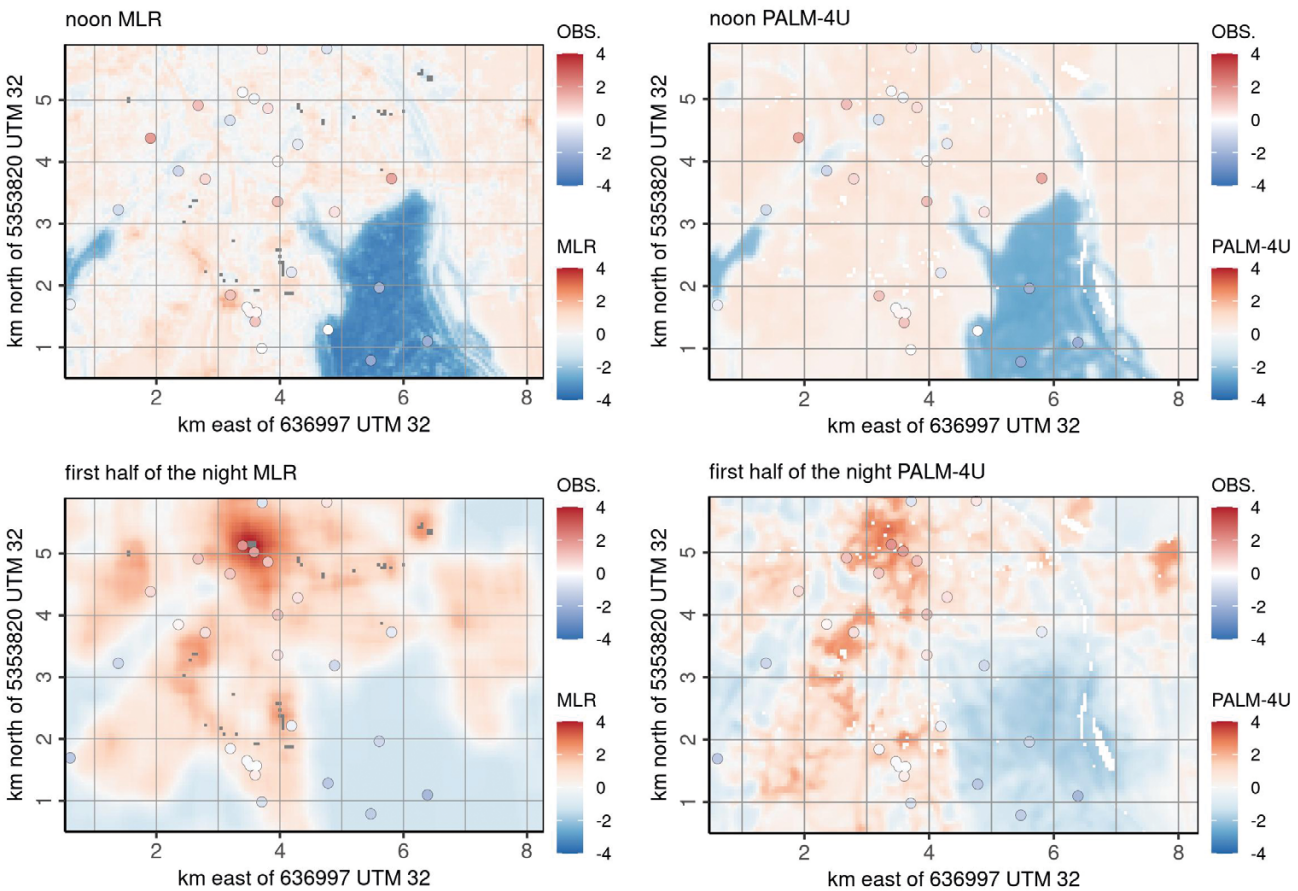

Fig. 5. Exemplary comparison of the maps of z-standardized theta from PALM-4U (cf. section 2.4) and the MLR for selected times of day, including theta derived from the T_{air} measurements of the stationary network. Coordinates are given in km from the south-western corner of the PALM-4U domain. Left: MLR, right: PALM-4U, above: noon, below: first half of the night.

maps, which is to be expected and is in line with many other studies (e.g., Balany et al. 2020; Jacobs et al. 2020). Theta is higher in the city centre, other built-up parts of the domain, and the open areas surrounding the city, but spatial differences are slight. The theta from the stationary measurement network also shows the lowest values in the forest and along the rivers. However, in the rest of the domain, they exhibit more considerable horizontal differences than the two model approaches. In the evening, the spatial variation in PALM-4U and the MLR increases, with a clear dependence on surface characteristics. Again, both model approaches show a good agreement. The measurements fit both maps better than at noon, with the highest theta in the inner-city, medium values towards the edges of built-up areas, and the lowest values in natural surroundings.

3.3 Analysis of hot- and coldspots

3.3.1 Location of hot- and coldspots

The results of the G_i* statistic for the PALM-4U simulation with dynamic forcing from COSMO-D2 of the heat day are presented in Fig. 6. Overall, the spatial distribution of hot- and coldspots follows surface characteristics. In the morning and noon, only a few street canyons are highly significant hotspots, but significant hotspots also occur in most of the built-up areas. Coldspots are restricted mainly to larger urban green spaces and forests but do not extend into the surroundings of these natural areas, which contradicts the studies by, e.g., Chang & Li (2014) and Li et al. (2021), where measurements revealed cooling effects in the surroundings of urban green spaces also during daytime. Most of the open areas and several inner-city points have insignificant G_i* values (Fig. 6b and 6c). In the evening, the area with highly significant hotspots increases distinctly and covers large parts of the built-up area of Augsburg. Besides, the area of some significant coldspots increases, too, e.g., around the forest (Fig. 6d). During the night, this distribution mostly stays the same. However, some hotspots become smaller, especially in the western part of the city. Besides, some inner-city green spaces, which are coldspots during the day, turn into hotspots at night (Fig. 6e and 6f) (see also section 4.2). Some considerable differences occur between the G_i* patterns of the second half of the night before and after the heat day in the study area (Fig. 6a and 6f). On the night before the heat day, there are mainly insignificant values of G_i* in the built-up area of the northern and north-western part of the area, and the coldspots around the forest expand farther into the built-up areas in its surroundings. On the other hand, after the heat day at night, there are several highly significant hotspots in the northern and north-western part of the domain, and the coldspot of the forest is smaller than during the night before the heat day. Differences also occur in the south-western part of the study area, with larger highly significant hotspots in the night before the heat day compared to the night after the heat day.

A comparison of the G_i* statistic from PALM-4U and MLR shows good agreement for some times of the day. At noon (Figs. 7a and 6c), both maps have only a few highly significant hotspots, which occur in the built-up part of the domain. Significant coldspots are mainly restricted to natural areas. In the evening (Figs. 7b and 6d), significant hotspots can be found in most of the built-up areas in both cases, and significant coldspots extend over the borders of natural areas. On the other hand, there are considerable differences in the G_i* maps from PALM-4U for the second half of the night before and after the heat day, as shown above (Figs. 6a and 6f). In the MLR, however, the relatively coarse classification of weather categories leads to the attribution of both nights to the same weather type, namely “calm and clear”. Therefore, the MLR produces the same G_i* map for both situations, which fits better with the PALM-4U pattern for the night after the heat day (Figs. 7c and 6f). There are considerable differences for the night before the heat day, thus at a time which can be expected to be clearly outside the spin-up interval of PALM-4U, especially in the eastern half of the domain (Figs. 7c and 6a). This indicates that even under calm conditions, the circulation influences spatial theta patterns in cities, which cannot be captured adequately by this MLR model.

3.3.2 Statistical analysis of hotspots from PALM-4U

This section presents the statistical analysis of unexpected hotspots and unexpectedly missing hotspots defined based on PALM-4U results and static variables as described in section 2.5 (Fig. 8), as well as their locations during the course of the day (Fig. 9).

The statistical analysis of meteorological variables for the expected and unexpected hotspots shows significant differences for several variables, as shown by the U-test (Fig. 8, red bars. For boxplots of the comparison the reader is referred to figures S1 and S2, red boxes). In general, unexpected hotspots are areas with reduced turbulence intensity, and lower vertical shear of horizontal wind speed compared to expected hotspots. Shear turbulence is, therefore, reduced. Higher horizontal wind speeds near the ground and within the canopy layer (which are very similar, see also figure S2, red boxes) but lower horizontal wind speeds above the canopy layer compared to expected hotspots for most times of day support the reduction of vertical shear of horizontal wind speed and, thus, the development of unexpected hotspots. Unexpected hotspots show higher absolute vertical wind speeds and higher lapse rate compared to expected hotspots and are characterized by increased incoming solar radiation and, especially at night, soil moisture is slightly higher. The relationship of sensible to latent heat flux shows, that for expected hotspots, sensible heat predominates, while in unexpected hotspots, evaporation is higher (Fig. 8, red bars). For unexpected hotspots, the mixing ratio is smaller as at expected hotspots most of the day. The unexpected hotspots are among the warmest areas during the second half of the

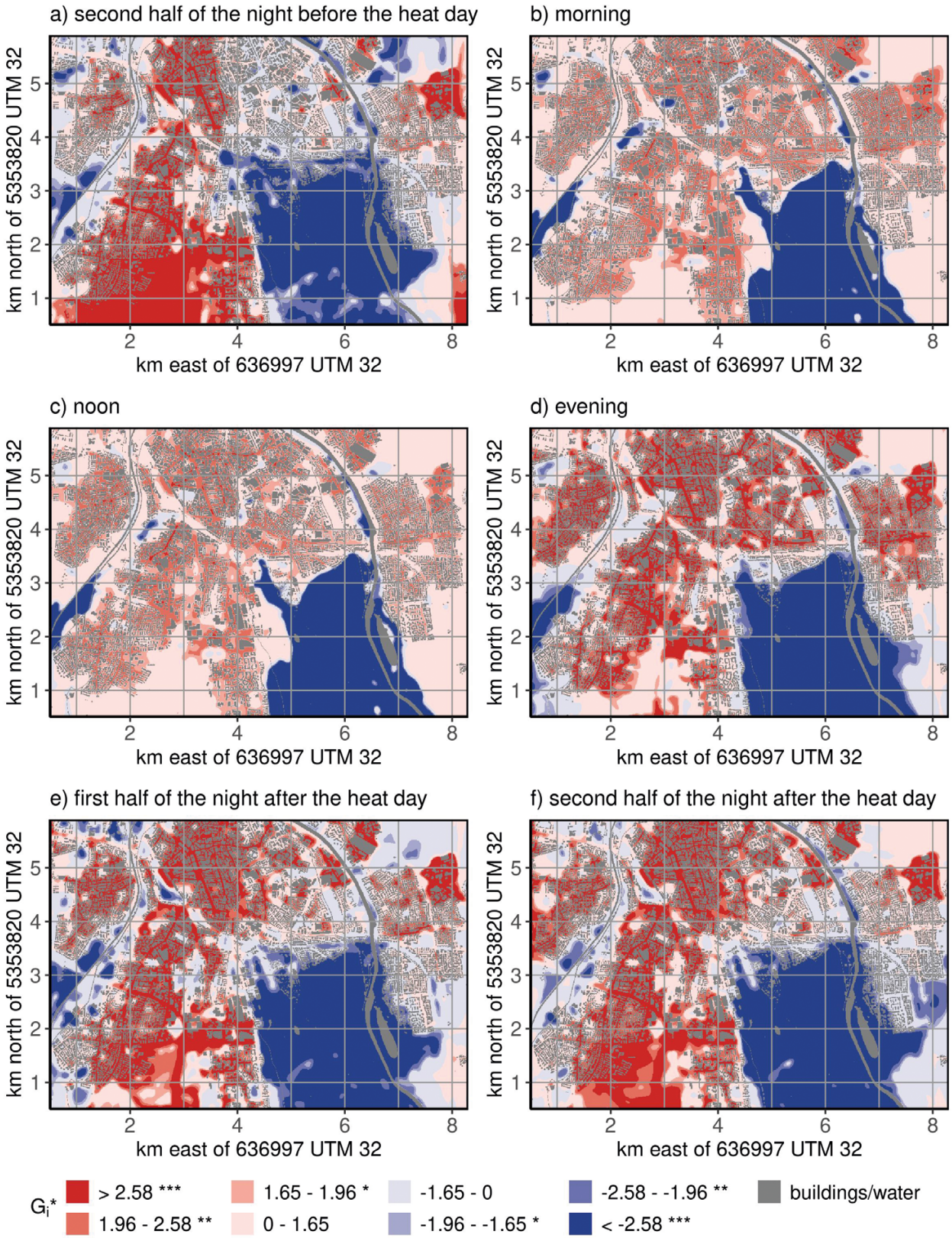

Fig. 6. Locations of hot- and coldspots from the PALM-4U simulation of the heat day given by the G_i* statistic, which detects local clusters of high or low values, respectively, by comparing regions and their surroundings to the mean value of the whole study area. Coordinates are given in km from the south-western corner of the PALM-4U domain. Symbols in the legend: ***=highly significant, **=very significant, *=significant, no symbol: insignificant.

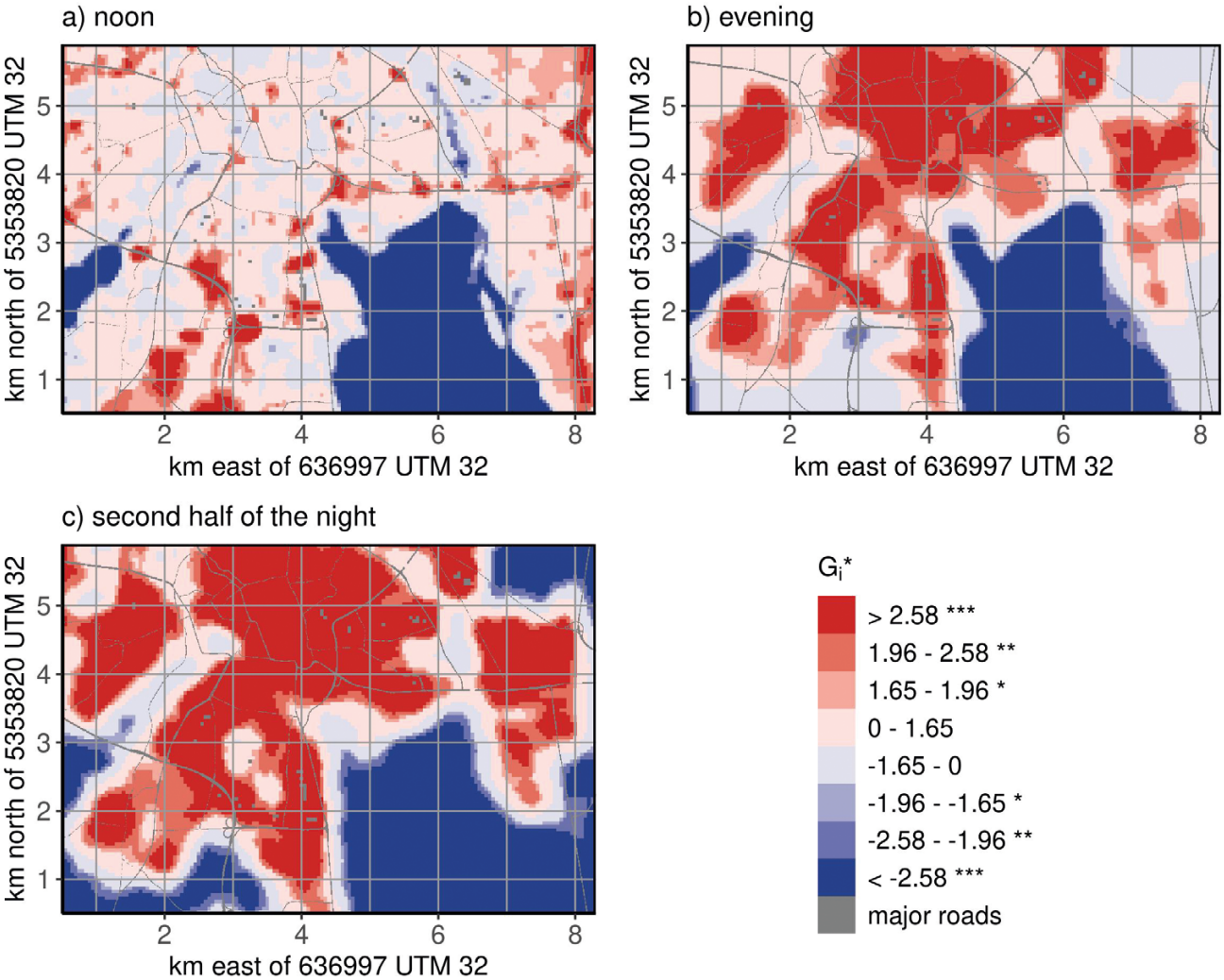

Fig. 7. Comparison of the locations of hot- and coldspots (given by the G_i* statistic) from MLR for selected times of the day. Coordinates are given in km from the south-western corner of the PALM-4U domain. Symbols in the legend: ***=highly significant, **=very significant, *=significant, no symbol: insignificant.

first night and in the morning but show slightly lower theta than expected hotspots in the noon and evening (figure S2, red boxes). The areas with unexpected hotspots comprise relatively open places throughout the day, including sometimes the edges of the built-up area. At night, they can also be found in some inner-city parks (Fig. 9).

Unexpectedly missing hotspots are characterized by higher horizontal wind speeds near the ground (figure S2, blue boxes) and in and above the canopy layer compared to other areas with insignificant G_i* or coldspots, i.e. other areas without hotspots (Fig. 8, blue bars. For boxplots of the comparison the reader is referred to figures S1 and S2, blue boxes). Besides, absolute vertical wind speeds and turbulence intensity also show increased values for most times of the day and the lapse rate is reduced, indicating a less stable thermal stratification in unexpectedly missing hotspots compared to other areas without hotspot. These all facilitate vertical mixing and transport. The differences in the vertical shear of horizontal wind speed between these two types of areas without hotspot vary over the course of the day, with increased values at noon and in the first half of the night, indicating increased turbulence. On the other hand, shortwave incoming radiation in unexpectedly missing hotspots is reduced and soil moisture is slightly lower compared to other areas without hotspot. In areas with unexpectedly missing hotspots, sensible heat flux is higher than in other areas without hotspot, where latent heat flux often exceeds (Fig. 8, blue bars). The areas with unexpectedly missing hotspots are mainly densely built-up areas. By day, many of them are located in the inner-city. They can mostly be found in the built-up areas near the forests, rivers, and green spaces in the evening and at night. On the night before the heat day, a noticeably large number of such areas is located in the eastern half of the built-up part of the study area (Fig. 9).

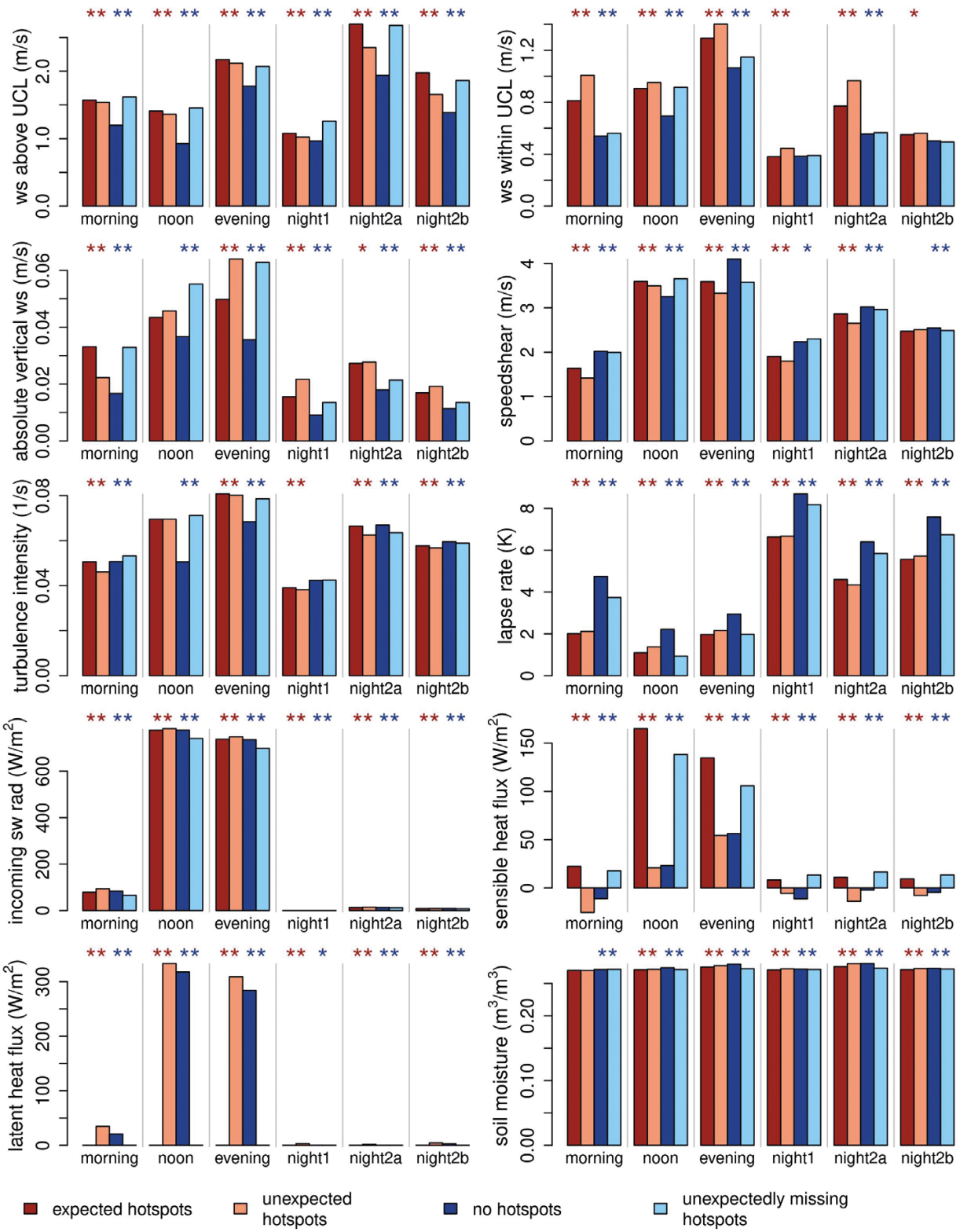

Fig. 8. Barplots comparing medians of different meteorological variables for expected and unexpected hotspots (dark and light red) as well as no hotspots and unexpectedly missing hotspots (dark and light blue) for different times of the day. Symbols above the plots show the level of significance of the U-test for the respective variable and time of day. **: α = 0.01, *: α = 0.05, ~: α = 0.1, no symbol: insignificant. Colours of the symbols indicate the types of hotspots which are compared: red symbol for the comparison of unexpected and expected hotspots, blue symbol for the comparison of no hotspots and unexpectedly missing hotspots. X-axis labels for the night: night1 = first half of the night, night2a = second half of the night before the heat day, night2b = second half of the night after the heat day. UCL = urban canopy layer, ws = wind speed, sw rad = shortwave radiation. Wind speeds are horizontal wind speeds if not indicated differently. Figure S1 gives the medians presented here as numbers.

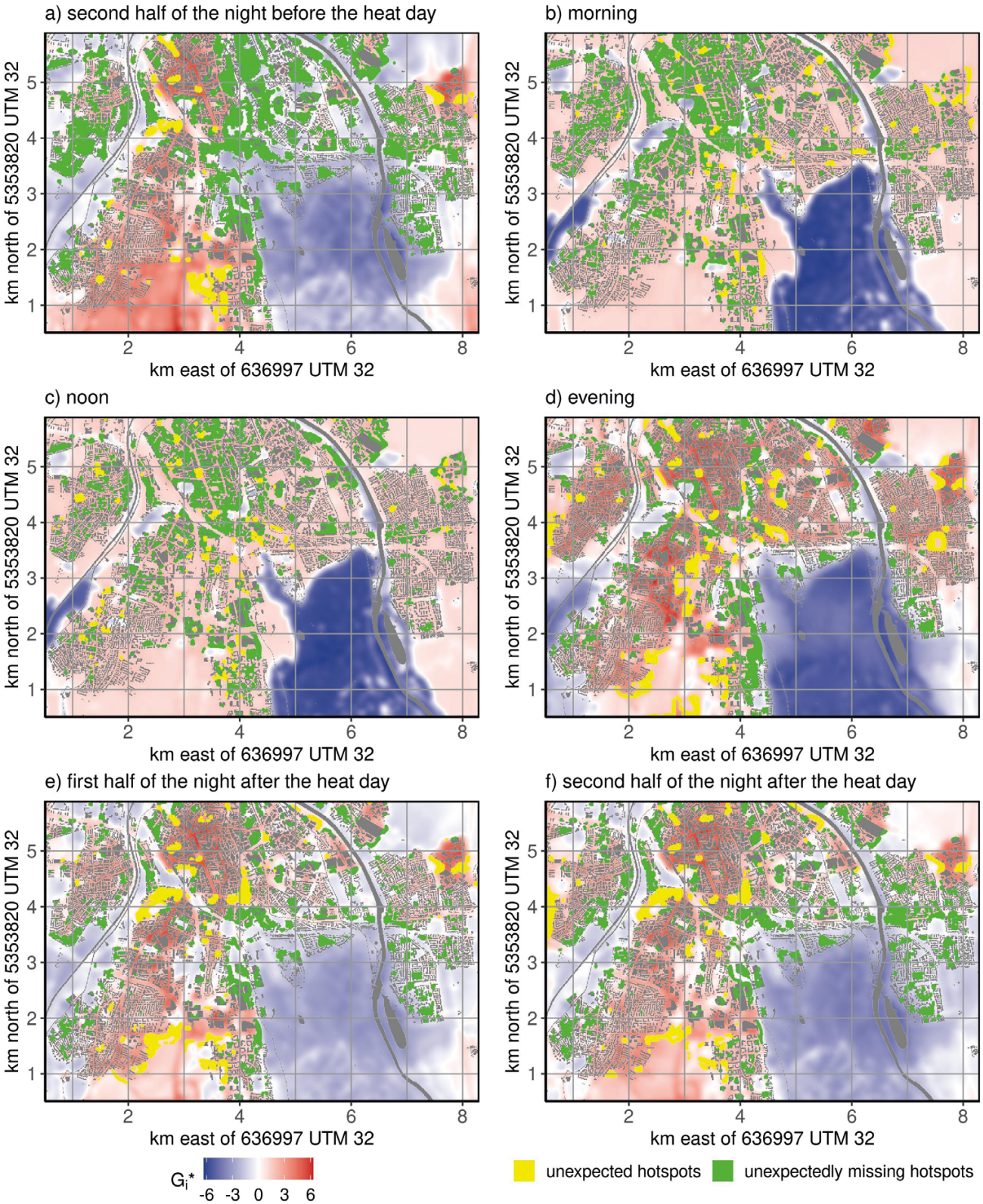

Fig. 9. Location of unexpected hotspots (yellow) and unexpectedly missing hotspots (green) for the different time intervals during the heat day. Coordinates are given in km from the south-western corner of the PALM-4U domain.

The analysis of trajectories (Fig. 10) shows that air with higher mean theta is transported towards the unexpected hotspots compared to the expected hotspots. This is true for all times of day. At night the air reaching unexpected hotspots is even warmer than the hotspot itself in many cases. Besides, the turbulence values of the incoming air are lower for unexpected than for the expected hotspots. Unexpectedly missing hotspots receive cooler air and less turbulence for most times of day compared to hotspots. Horizontal wind speeds influence the length of the trajectories. They are higher for unexpected hotspots than for expected and missing hotspots, especially during the second half of the first night and during the day. Thus, the air comes from a larger surrounding area. Wind speeds also influence the amount of adaptation of a moving air parcel to the underlying surfaces. The mean height above ground of the advected air parcels is lower for unexpected hotspots for some times of day compared to expected hotspots, indicating less vertical temperature flux.

4 Discussion

4.1 Comparison of PALM-4U and MLR

Overall, the comparison between the theta fields from PALM-4U and the MLR shows good agreement for most of the simulated period. This also applies to the G_i* fields from the two models. Consequently, surface characteristics play an essential role in the development of spatial theta patterns in both approaches, which has already been shown by many studies relating land use and land cover to urban air or surface temperatures (e.g., Oke 1982; Kottmeier et al. 2007; Fenner et al. 2017; Siqi & Yuhong 2020; Burger et al. 2021).

However, there are differences in the correlation between the theta fields from both models over the day, and the agreement of the G_i* maps varies, too. For the second half of the night before the heat day, the lowest correlations between PALM-4U and MLR were obtained. A reason could be the slightly higher wind speed on the first night compared to the rest of the studied period. In the MLR, the first night is within the class “clear and calm” and, thus, assumes the same synoptic conditions as the other times of the day. In the PALM-4U theta fields, however, a distinctly different pattern is visible, which results from the different wind conditions. The mean horizontal wind speed near the ground in the PALM-4U domain during the second half of the night before the heat day amounts to 3.5 m/s to 4.5 m/s. With a maximum extent of built-up area in the domain of approximately 7.2 km, the air parcels pass this area within approximately 25 to 35 minutes. In addition, it should be noted that the most densely built-up part of the city is even smaller, leading to less time of contact between passing air and these surfaces. Therefore, warm air is removed efficiently and the influence of land use/land cover variables on theta is reduced in PALM-4U in this situation. Furthermore, the wind direction is not taken into account in the MLR model at all but is modelled in PALM-4U explicitly. Another reason for differences could be the critical influence of incoming shortwave radiation by day, which is included in PALM-4U via a radiative transfer model (Krč et al. 2021). In the MLR, however, such effects cannot be modelled. The SVF is the only predictor variable related to radiation effects. However, it does not include information about the exact geometry and orientation of street canyons, which influences shadowing, nor any other mechanisms that the radiative transfer model calculates.

In principle urban landcover is heterogeneous across different length-, magnitude-, and timescales. Therefore, accurate predictions require non-local state- and transport information to a larger extent compared to homogeneous surfaces. While we accounted for spatial variance in our MLR model approach, the transport component is generalized homogeneously by defining a circle of influence. This simplification limits the MLR model’s representativeness, as features that depend on transport direction (i.e., advection) are underrepresented.

Consequently, it seems essential to take wind speed, wind direction, and building geometry into account in model approaches. Barlow et al. (2008) also emphasize the dependence of urban features, in their case roughness parameters, on flow direction. Minor differences in the large- and mesoscale meteorological situation influence the theta patterns calculated by PALM-4U, and being able to model such individual situations is a strength of microscale models.

4.2 Circulation effects on the occurrence and absence of hotspots

The positions and temporal development of hot- and coldspots in the PALM-4U theta patterns are often related closely to surface characteristics, which is in line with many other studies, as shown in section 4.1. The statistical analysis shows that unexpected hotspots are characterized by higher incoming shortwave radiation, which indicates missing shadowing effects, presumably due to the specific building geometry. This also shows the critical influence of land use/land cover characteristics on theta. In order to focus on the different factors responsible for causing unexpected and unexpectedly missing hotspots, the characteristics of unexpected hotspots are compared to expected hotspots and the characteristics of unexpectedly missing hotspots are compared to other areas without hotspot. This analysis of unexpected hotspots and areas where hotspots would be expected but are missing indicates that the circulation can explain deviations from the relation of land use/land cover characteristics and theta.

The unexpected hotspots are areas with higher horizontal wind speeds in the canopy layer, but lower wind speeds above compared to the expected hotspots. This indicates that advection, transporting warmer air from the surroundings to these spots, plays a role. In addition, the higher vertical wind speeds and higher lapse rate in unexpected hotspots compared to expected hotspots can be explained by enhanced

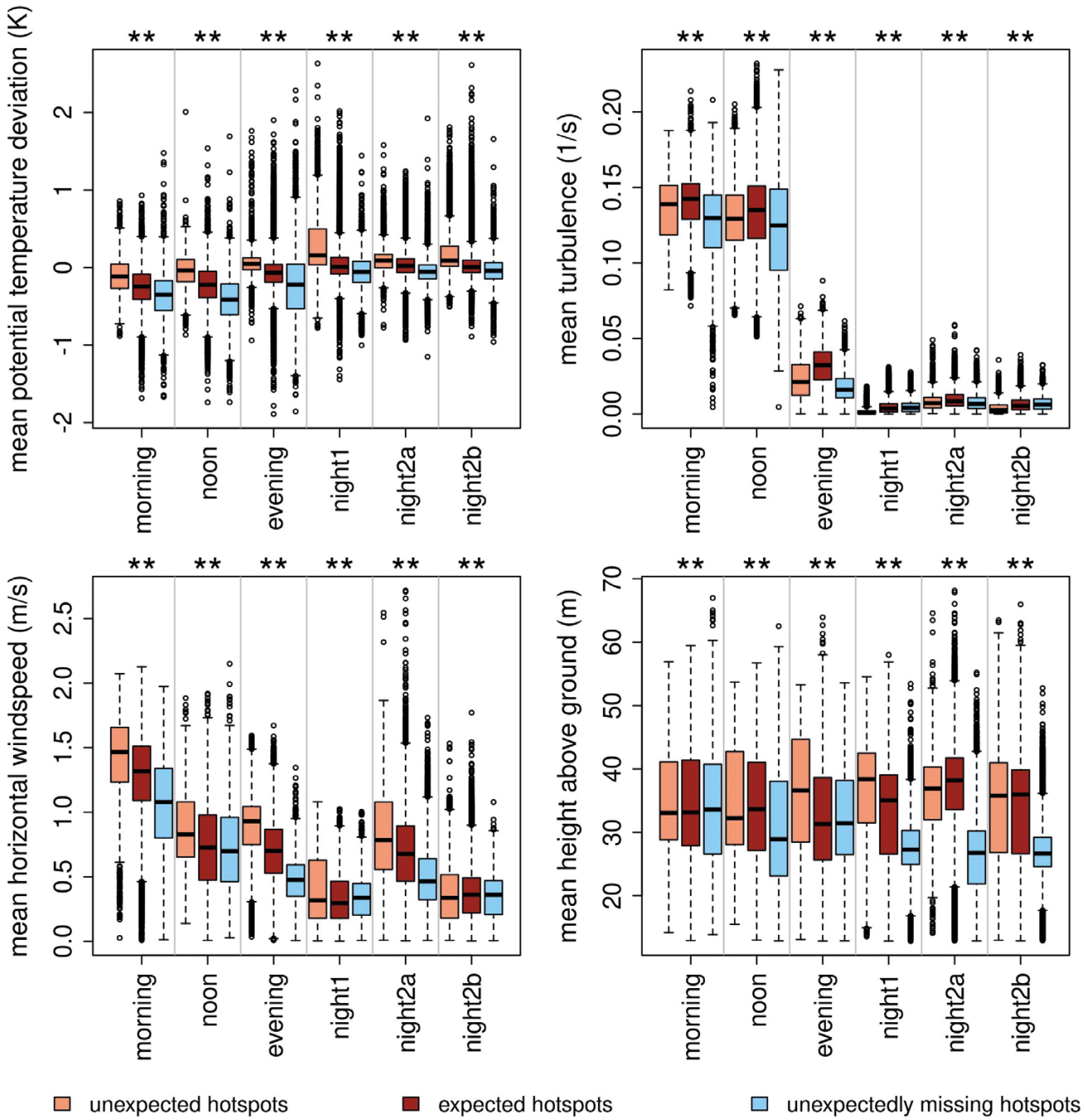

Fig. 10. Boxplots for the comparison of different variables for the 5-minute trajectories for unexpected hotspots, expected hotspots and unexpectedly missing hotspots. The symbols above the plots indicate the level of significance of the Kruskal-Wallis test for the respective variable and time of day. Symbols above the plots and x-axis labels are defined as in Fig. 8, boxplots are defined as in Fig. 3. Mean deviation of potential temperature in the upper left panel refers to the difference of potential temperature of the trajectory and the respective hotspot/missing hotspot.

convection at unexpected hotspots associated with low level advection towards the convection centre. Gedzelman et al. (2003) and Vicente-Serrano et al. (2005) show that the UHI can shift its position due to variations in the wind direction, so the influence of wind relocates the warmer areas. Brousse et al. (2022) show that horizontal advection of heat is also an essential factor at the scale of LCZs in urban areas. Such effects can be explained by the thermally induced urban breeze circulation or urban heat island circulation (e.g., Wong & Dirks 1978; Hidalgo et al. 2008; Hong et al. 2024), which develops strongest under calm background winds near the ground. Similar processes can play a role on the microscale,

as in the case of Augsburg. The analysis of trajectories confirms that unexpected hotspots receive warm air with small turbulence signals compared to other locations. In addition, turbulence and vertical exchange are significantly reduced in locations of unexpected hotspots. This means that by day, the warm air near the ground is mixed less with cooler air from above the canopy layer, which prevents a cooling effect in the canopy layer. The mean height of the trajectories can be interpreted as an indirect indicator for vertical transport, because in the case of trajectories passing high altitudes and ending at ground level, vertical winds enable air parcels to be transported from higher levels to the near surface atmosphere, where the hotspots are defined. On the other hand, the height of the tracks can also be a result of the building height in the respective area. However, together with the turbulence intensity of the advected air, the results confirm the tendency that air arriving at unexpected hotspots is not mixed vertically to the same extent as air reaching expected hotspots. The slightly higher soil moisture found at unexpected hotspots is as expected due to the more natural surface types and underlines the importance of atmospheric advection. The unexpected hotspots found at night under the trees in inner-city parks could result from reduced longwave emission due to small sky view factors (Spronken-Smith & Oke 1999) as well as reduced wind speed due to increased roughness and, thus, reduced exchange of air masses (Shahidan 2015; Yuan et al. 2017). According to Foken (2006), forests can be warmer than their surroundings in the evening, and at night, warming can occur due to gusts that transport warm air from the crowns toward the ground. Small parks, in particular, can be warm compared to their surroundings under some conditions (e.g., Chang et al. 2007). The differences of ground heat flux, sensible and latent heat flux between expected and unexpected hotspots are small. Although there are differences in the medians, the overall distributions are very similar. Therefore, these variables were not examined in more detail.

For the areas where hotspots are missing unexpectedly, higher horizontal wind speeds in and above the canopy layer were found compared to areas where hotspots are not expected. Here, an advection of air could also play a role, but in this case, the air is assumed to originate from natural surroundings and cool the built-up areas. The analysis of trajectories shows the advection of relatively cool air towards unexpectedly missing hotspots and confirms this assumption. This is in line with the fact that these built-up areas are mainly near the forest, rivers, or inner-city parks in the evening and night and can be explained by the park cool island effect (e.g., Spronken-Smith & Oke 1998). Its impact can be observable at a considerable distance from the green space (e.g., Upmanis et al. 1998; Yan et al. 2018; Algretawee 2022). The importance of advection for the cooling of densely built urban areas on a regional scale is also highlighted by Steigerwald et al. (2022). In addition, the turbulence intensity is increased in these spots most of the day. This indicates effective mixing, which can contribute to the cooling of these areas.

These results indicate that even in situations with low wind speeds, horizontal and vertical circulation significantly impact the locations with the highest temperatures in a city. This study only focuses at one specific day within a heat wave but already shows that different theta patterns can occur in situations classified into the same weather type. Therefore, accounting for the individual circulation patterns, which are highly variable, is essential. Consequently, it would be necessary to run many PALM-4U simulations for different conditions to cover the spread of possible spatial hotspot distributions. Such a catalogue approach is used in the GRAMM-GRAL model (e.g., Berchet et al. 2017).

Furthermore, differences in the large- and mesoscale circulation could contribute to the different patterns in the first and second nights of the studied period. Such effects should be studied in more detail.

For urban planning, these results show the importance of taking different flow conditions and weather types instead of selected days or mean conditions into account to gain more accurate information on the locations of the warmest areas because high ambient temperatures favour heat stress for humans. In order to implement the various heat adaptation measures as efficiently as possible, this would be necessary to ensure quality of life and minimize health risks due to heat stress in cities in the future. On the other hand, the effort required to simulate many different situations with a microscale model is extensive and is only feasible for some city administrations. Therefore, the practicability of such an approach needs to be investigated. Simulating smaller domains in PALM-4U or applying the model without self-nesting is an option for reducing the necessary resources for the computation.

4.3 Limitations

Some limitations of the study concern the PALM-4U setup.

The water surface temperature in the PALM-4U simulations is set to a fixed value. Thus, it does not exhibit a daily cycle. In this study, the default value of 285 K was used, which is too cold for a summer day. Measurements of the surface temperature of the river Lech in Augsburg show values between 17.5 °C and 19 °C for the simulated day (Gewässerkundlicher Dienst Bayern 2024). Consequently, the cooling effect of water surfaces is likely to be overestimated in the PALM-4U model results. Such measured values should be taken into account for an improvement of the model setup.

Further limitations of the PALM-4U simulations relate to the static and dynamic input data. In the static driver, different sources of information are combined to describe the land surface and land cover. Some variables were derived from the crowdsourcing project Open Street Map. Studies have found good completeness and considerable agreement between Open Street Map data and commercial and official

data sets for Germany (Neis et al. 2011; Dorn et al. 2015). Thus, the data quality of Open Street Map can be regarded as reliable, especially in urban areas. However, errors and missing data can occur. The data from official sources can be assumed to be reliable. However, these data sets are updated infrequently, so errors can still occur. For example, a few newer buildings were missing in the building model data. Such errors or missing features can affect the PALM-4U results, e.g., by modification of the flow, the turbulence, and the energy balance, at least locally. Uncertainties in the land cover data may also affect the MLR model (see also Straub et al. 2019). Further uncertainties result from setting a uniform soil type in the whole PALM-4U domain, which may affect the calculation of soil moisture, but due to the lack of more detailed information, assumptions had to be made. However, for Augsburg, a medium-fine soil type is assumed to be a good approximation, because of the occurrence of luvisols and mixed rendzinas in the surroundings of the PALM-4U model domain (Bayerisches Geologisches Landesamt 1987). Collecting more detailed soil data in cities and making them publicly available could help improve the setup of microscale urban models. The dynamic driver from a mesoscale model provides meteorological input at the model boundaries. It was found that PALM-4U is very sensitive towards dynamic forcing, which is in line with the results from Vogel et al. (2022). In the current study, this is a primary factor leading to theta values that are too low in PALM-4U compared to measurements.

Other problems may result from the spatial resolution of the PALM-4U domain. The evaluation of vertical theta profiles indicates that PALM-4U does not fully resolve the turbulence at night and underestimates the height of the inversion at some time steps. Therefore, the resolution of 10 m could be too coarse. On the other hand, a compromise between the resources needed for one simulation and a high resolution always has to be made. While compute resources are increasingly available, rising energy prices led to the emergence of ideas about sustainable computing and increasing interest in optimization and feasibility.

The utilization of potential temperatures instead of T_{air} for the PALM-4U evaluation and hotspot analysis as well as the utilization of air pressure measurements from the DWD station for the calculation of theta and mixing ratios for the THL and AWS leads to uncertainties due to altitude differences in the study area and dynamic pressure fluctuations. The dynamic pressure fluctuations represented by the perturbation pressure calculated by PALM-4U are very small and, therefore, lead only to small uncertainties regarding theta (maximum 0.16 K). The altitude differences in the study area amount to a maximum of 35 m, which corresponds to uncertainties of calculated theta of up to 0.37 K. Small scale air pressure differences estimated by the air pressure difference between the DWD station and the AWS at the University of Augsburg amount to 4.5 hPa for the studied day, which corresponds to a theta difference of 0.41 K, while 0.53 K can be attributed to the altitude difference of approximately 50 m between the two sites. These theta uncertainties are distinctly smaller than the theta differences between significant hot- and coldspots and areas with insignificant G_i* (cf. table S1). Therefore, for Augsburg, the spatial theta patterns seem to give a good approximation of T_{air} patterns but the cooler areas of significant hotspots and the warmer areas of significant coldspots, especially at higher altitudes, have to be interpreted with care. For a more straightforward approach, the hotspot analysis could be conducted with the T_{air} calculated from the PALM-4U output and for assessing human heat stress, it could be repeated with output variables from the PALM-4U biometeorology module. Furthermore, for the PALM-4U evaluation, uncertainties due to the calculation of theta and mixing ratios based on air pressure measurements from the DWD station can lead to an underestimation of the bias.

5 Summary and conclusion

This study investigated the spatio-temporal distribution of urban theta hot- and coldspots during a summerly heat wave in the medium-sized city of Augsburg. Microscale simulations with the LES model PALM-4U and a statistical MLR model were utilized to gain insight into these patterns for different times of the day. The main result was that in addition to the well-studied impact of land use and land cover on urban temperature patterns, different variables related to the circulation are important. Horizontal wind speed, which causes horizontal advection, was one main factor connected to unexpected theta patterns. Turbulence, vertical exchange and advection of air masses have a significant influence, too. Reduced turbulence promotes the development of unexpected hotspots, while increased turbulence prevents the development of hotspots. These processes were effective even under low mesoscale wind speeds when urban air temperature patterns are often assumed to depend mainly on surface characteristics. The manifestation of these processes under different synoptic conditions remains an open question because only one specific day was investigated in this study. However, the indicated prominent role of circulation suggests that assessments of distribution and intensity of urban hotspots based on single simulations for a distinct synoptic situation may be limited and may be improved by consideration of a multitude of different typical weather types leading to varying influences of small-scale circulation. The role of circulation compared to surface characteristics for the establishment of urban cold spots, which might also play an important role for human health, should be also addressed in more detail in the future, in order to improve urban planning, where the effective implementation of heat mitigation measures is a major goal.

Funding: This research project is funded by the Federal Ministry of Education and Research (BMBF) in the scope of the BMBF Programme Urban Climate Under Change [UC]².

Acknowledgements: The authors would like to thank Alexandra Schneider, Kathrin Wolf and Josef Cyrys (Helmholtz Zentrum München, Institute of Epidemiology, Research Groups "Environmental Risks" and "Exposure Assessment") for supporting the study with outdoor air temperature data from the cooperative urban meteorological network (HOBO loggers) in Augsburg, which was set up as a cooperative effort of Helmholtz Zentrum München, Institute of Epidemiology and the University of Augsburg, Institute of Geography.

The authors would like to thank the anonymous reviewers for the valuable comments and suggestions on the manuscript, which helped to improve this paper.

Data availability statement: Data from the HOBO logger network as well as the PALM-4U model output will be made available on request. Data from the automatic weather stations (Reinhardt stations), the vertical UAS measurements and relevant subsets of the PALM-4U model output are going to be made available publicly under https://climate.geo.uni-augsburg.de/hotspots-augsburg-2025.

References

Alcoforado, M.-J., & Andrade, H. (2006). Nocturnal urban heat island in Lisbon (Portugal): Main features and modelling attempts. *Theoretical and Applied Climatology, 84*(1), 151–159. https://doi.org/10.1007/s00704-005-0152-1

Algretawee, H. (2022). The effect of graduated urban park size on park cooling island and distance relative to land surface temperature (LST). *Urban Climate, 45*, 101255. https://doi.org/10.1016/j.uclim.2022.101255

Anders, J., Schubert, S., Sauter, T., Tunn, S., Schneider, C., & Salim, M. (2023). Modelling the impact of an urban development project on microclimate and outdoor thermal comfort in a mid-latitude city. *Energy and Building, 296*, 113324. https://doi.org/10.1016/j.enbuild.2023.113324

Arnfield, A. J. (2003). Two decades of urban climate research: A review of turbulence, exchanges of energy and water, and the urban heat island. *International Journal of Climatology, 23*(1), 1–26. https://doi.org/10.1002/joc.859

Balany, F., Ng, A. W., Muttil, N., Muthukumaran, S., & Wong, M. S. (2020). Green Infrastructure as an Urban Heat Island Mitigation Strategy – A Review. *Water (Basel), 12*(12), 3577. https://doi.org/10.3390/w12123577

Barlow, J. F., Rooney, G. G., von Hünerbein, S., & Bradley, S. G. (2008). Relating Urban Surface-layer Structure to Upwind Terrain for the Salford Experiment (Salfex). *Boundary-Layer Meteorology, 127*(2), 173–191. https://doi.org/10.1007/s10546-007-9261-y

Bayerisches Geologisches Landesamt (1987). Standortkundliche Bodenkarte von Bayern 1:50000, L7730 Augsburg. München.

Beck, C., Straub, A., Breitner, S., Cyrys, J., Philipp, A., Rathmann, J., … Jacobeit, J. (2018). Air temperature characteristics of local climate zones in the Augsburg urban area (Bavaria, southern Germany) under varying synoptic conditions. *Urban Climate, 25*, 152–166. https://doi.org/10.1016/j.uclim.2018.04.007

Berchet, A., Zink, K., Oettl, D., Brunner, J., Emmenegger, L., & Brunner, D. (2017). Evaluation of high-resolution GRAMM–GRAL (v15.12/v14.8) NO_x simulations over the city of Zürich, Switzerland. *Geoscientific Model Development, 10*(9), 3441–3459. https://doi.org/10.5194/gmd-10-3441-2017

Bivand, R. S., & Wong, D. W. S. (2018). Comparing implementations of global and local indicators of spatial association. *Test, 27*(3), 716–748. https://doi.org/10.1007/s11749-018-0599-x

Brousse, O., Simpson, C., Walker, N., Fenner, D., Meier, F., Taylor, J., & Heaviside, C. (2022). Evidence of horizontal urban heat advection in London using six years of data from a citizen weather station network. *Environmental Research Letters, 17*(4), 044041. https://doi.org/10.1088/1748-9326/ac5c0f

Bruns, J., & Simko, V. (2017). Stable Hotspot Analysis for Intra-Urban Heat Islands. *GI Forum, 1*, 79–92.

Burger, M., Gubler, M., Heinimann, A., & Brönnimann, S. (2021). Modelling the spatial pattern of heatwaves in the city of Bern using a land use regression approach. *Urban Climate, 38*, 100885. https://doi.org/10.1016/j.uclim.2021.100885

Cao, J., Zhou, W., Zheng, Z., Ren, T., & Wang, W. (2021). Within-city spatial and temporal heterogeneity of air temperature and its relationship with land surface temperature. *Landscape and Urban Planning, 206*, 103979. https://doi.org/10.1016/j.landurbplan.2020.103979

Chang, C.-R., & Li, M.-H. (2014). Effects of urban parks on the local urban thermal environment. *Urban Forestry & Urban Greening, 13*(4), 672–681. https://doi.org/10.1016/j.ufug.2014.08.001

Chang, C.-R., Li, M.-H., & Chang, S.-D. (2007). A preliminary study on the local cool-island intensity of Taipei city parks. *Landscape and Urban Planning, 80*(4), 386–395. https://doi.org/10.1016/j.landurbplan.2006.09.005

Dilley, A. C., & O'Brien, D. M. (1998). Estimating downward clear sky long-wave irradiance at the surface from screen temperature and precipitable water. *Quarterly Journal of the Royal Meteorological Society, 124*(549), 1391–1401.

Dorn, H., Törnros, T., & Zipf, A. (2015). Quality Evaluation of VGI Using Authoritative Data – A Comparison with Land Use Data in Southern Germany. *ISPRS International Journal of Geo-Information, 4*(3), 1657–1671. https://doi.org/10.3390/ijgi4031657

Dutilleul, P., Clifford, P., Richardson, S., & Hemon, D. (1993). Modifying the t Test for Assessing the Correlation Between Two Spatial Processes. *Biometrics, 49*(1), 305–314. https://doi.org/10.2307/2532625

DWD Climate Data Center (2024a). Hourly station observations of 2 m air temperature and humidity for Germany, Version v24.03. ftp://opendata.dwd.de/climate_environment/CDC/. Accessed: 2024-10-01.

DWD Climate Data Center (2024b). Hourly station observations of pressure for Germany, Version v24.03. ftp://opendata.dwd.de/climate_environment/CDC/. Accessed: 2024-10-01.

Fan, Y., Li, Y., Bejan, A., Wang, Y., & Yang, X. (2017). Horizontal extent of the urban heat dome flow. *Scientific Reports, 7*(1), 11681. https://doi.org/10.1038/s41598-017-09917-4

Fenner, D., Meier, F., Bechtel, B., Otto, M., & Scherer, D. (2017). Intra and inter 'local climate zone' variability of air temperature as observed by crowdsourced citizen weather stations in Berlin, Germany. *Meteorologische Zeitschrift, 26*(5), 525–547. https://doi.org/10.1127/metz/2017/0861

Foken, T. (2006). *Angewandte Meteorologie – Mikrometeorologische Methoden*. Springer, Berlin, Heidelberg, 2 edition.

García, D. H., & Díaz, J. A. (2023). Space–time analysis of the earth's surface temperature, surface urban heat island and urban hotspot: Relationships with variation of the thermal field in Andalusia (Spain). *Urban Ecosystems, 26*(2), 525–546. https://doi.org/10.1007/s11252-022-01321-9

Gasparrini, A., & Armstrong, B. (2011). The impact of heat waves on mortality. *Epidemiology, 22*(1), 68–73. https://doi.org/10.1097/EDE.0b013e3181fdcd99

Gedzelman, S. D., Austin, S., Cermak, R., Stefano, N., Partridge, S., Quesenberry, S., & Robinson, D. A. (2003). Mesoscale aspects of the Urban Heat Island around New York City. *Theoretical and Applied Climatology, 75*(1), 29–42. https://doi.org/10.1007/s00704-002-0724-2

Geletič, J., Lehnert, M., Krč, P., Resler, J., & Krayenhoff, E. S. (2021). High-Resolution Modelling of Thermal Exposure during a Hot Spell: A Case Study Using PALM-4U in Prague, Czech Republic. *Atmosphere, 12*(2), 175. https://doi.org/10.3390/atmos12020175

Getis, A. & Ord, J. K. (1996). Local spatial statistics: an overview. In P. Longley & M. Batty (ed.), *Spatial Analysis: Modelling in a GIS Environment*, (pp. 261–277). Canada: Wiley & Sons.

Gewässerkundlicher Dienst Bayern (2024). Master data Augsburg Hochablaß. https://www.gkd.bayern.de/en/rivers/watertemperature/kelheim/augsburg-hochablass-12004002/total-period/table. Accessed: 2024-03-14.

Guerri, G., Crisci, A., Messeri, A., Congedo, L., Munafò, M., & Morabito, M. (2021). Thermal Summer Diurnal Hot-Spot Analysis: The Role of Local Urban Features Layers. *Remote Sensing, 13*(3), 538. https://doi.org/10.3390/rs13030538

Hamdi, R., Kusaka, H., Doan, Q.-V., Cai, P., He, H., Luo, G., … Termonia, P. (2020). The State-of-the-Art of Urban Climate Change Modeling and Observations. *Earth Systems and Environment, 4*(4), 631–646. https://doi.org/10.1007/s41748-020-00193-3

Heldens, W., Burmeister, C., Kanani-Sühring, F., Maronga, B., Pavlik, D., Sühring, M., … Esch, T. (2020). Geospatial input data for the PALM model system 6.0: Model requirements, data sources and processing. *Geoscientific Model Development, 13*(11), 5833–5873. https://doi.org/10.5194/gmd-13-5833-2020

Hidalgo, J., Pigeon, G., & Masson, V. (2008). Urban-breeze circulation during the CAPITOUL experiment: Observational data analysis approach. *Meteorology and Atmospheric Physics, 102*(3), 223–241. https://doi.org/10.1007/s00703-008-0329-0

Hong, S.-H., Jin, H.-G., & Baik, J.-J. (2024). Impacts of background wind on the interactions between urban breeze circulation and convective cells: Ensemble large-eddy simulations. *Quarterly Journal of the Royal Meteorological Society, 150*(760), 1518–1537. https://doi.org/10.1002/qj.4657

Hsu, C.-Y., Ng, U.-C., Chen, C.-Y., Chen, Y.-C., Chen, M.-J., Chen, N.-T., … Wu, C.-D. (2020). New land use regression model to estimate atmospheric temperature and heat island intensity in Taiwan. *Theoretical and Applied Climatology, 141*(3), 1451–1459. https://doi.org/10.1007/s00704-020-03286-1

Jacobs, C., Klok, L., Bruse, M., Cortesão, J., Lenzholzer, S., & Kluck, J. (2020). Are urban water bodies really cooling? *Urban Climate, 32*, 100607. https://doi.org/10.1016/j.uclim.2020.100607

Kadasch, E., Sühring, M., Gronemeier, T., & Raasch, S. (2021). Mesoscale nesting interface of the PALM model system 6.0. *Geoscientific Model Development, 14*(9), 5435–5465. https://doi.org/10.5194/gmd-14-5435-2021

Karttunen, S., Kurppa, M., Auvinen, M., Hellsten, A., & Järvi, L. (2020). Large-eddy simulation of the optimal street-tree layout for pedestrian-level aerosol particle concentrations – A case study from a city-boulevard. *Atmospheric Environment: X, 6*, 100073. https://doi.org/10.1016/j.aeaoa.2020.100073

Kim, S. W., & Brown, R. D. (2021). Urban heat island (UHI) variations within a city boundary: A systematic literature review. *Renewable & Sustainable Energy Reviews, 148*, 111256. https://doi.org/10.1016/j.rser.2021.111256

Knote, C., Hodzic, A., & Jimenez, J. L. (2015). The effect of dry and wet deposition of condensable vapors on secondary organic aerosols concentrations over the continental US. *Atmospheric Chemistry and Physics, 15*(1), 1–18. https://doi.org/10.5194/acp-15-1-2015

Kottek, M., Grieser, J., Beck, C., Rudolf, B., & Rubel, F. (2006). World Map of the Köppen-Geiger climate classification updated. *Meteorologische Zeitschrift (Berlin), 15*(3), 259–263. https://doi.org/10.1127/0941-2948/2006/0130

Kottmeier, C., Biegert, C., & Corsmeier, U. (2007). Effects of Urban Land Use on Surface Temperature in Berlin: Case Study. *Journal of Urban Planning and Development, 133*(2), 128–137. https://doi.org/10.1061/(ASCE)0733-9488(2007)133:2(128)

Kovats, R. S., & Hajat, S. (2008). Heat stress and public health: A critical review. *Annual Review of Public Health, 29*(1), 41–55. https://doi.org/10.1146/annurev.publhealth.29.020907.090843

Krč, P., Resler, J., Sühring, M., Schubert, S., Salim, M. H., & Fuka, V. (2021). Radiative Transfer Model 3.0 integrated into the PALM model system 6.0. *Geoscientific Model Development, 14*(5), 3095–3120. https://doi.org/10.5194/gmd-14-3095-2021

Kuttler, W., & Weber, S. (2023). Characteristics and phenomena of the urban climate. *Meteorologische Zeitschrift, 32*(1), 15–47. https://doi.org/10.1127/metz/2023/1153

Lai, D., Liu, W., Gan, T., Liu, K., & Chen, Q. (2019). A review of mitigating strategies to improve the thermal environment and thermal comfort in urban outdoor spaces. *The Science of the Total Environment, 661*, 337–353. https://doi.org/10.1016/j.scitotenv.2019.01.062

Li, Y., Fan, S., Li, K., Zhang, Y., Kong, L., Xie, Y., & Dong, L. (2021). Large urban parks summertime cool and wet island intensity and its influencing factors in Beijing, China. *Urban Forestry & Urban Greening, 65*, 127375. https://doi.org/10.1016/j.ufug.2021.127375

Lin, D., Khan, B., Katurji, M., Bird, L., Faria, R., & Revell, L. E. (2021). WRF4PALM v1.0: A mesoscale dynamical driver for the microscale PALM model system 6.0. *Geoscientific Model Development, 14*(5), 2503–2524. https://doi.org/10.5194/gmd-14-2503-2021

Maronga, B., Banzhaf, S., Burmeister, C., Esch, T., Forkel, R., Fröhlich, D., … Raasch, S. (2020). Overview of the PALM model system 6.0. *Geoscientific Model Development, 13*(3), 1335–1372. https://doi.org/10.5194/gmd-13-1335-2020

Masson, V., Lemonsu, A., Hidalgo, J., & Voogt, J. (2020). Urban Climates and Climate Change. *Annual Review of Environment and Resources, 45*(1), 411–444. https://doi.org/10.1146/annurev-environ-012320-083623

Mayer, S., Hattenberger, G., Brisset, P., Jonassen, M. O., & Reuder, J. (2012). A 'No-Flow-Sensor' Wind Estimation Algorithm for Unmanned Aerial Systems. *International Journal of Micro Air Vehicles, 4*(1), 15–29. https://doi.org/10.1260/1756-8293.4.1.15

Merkenschlager, C., Hertig, E., Simon, J., & Beck, C. (2023). High-resolution intra-urban assessments of future heat events and heat

waves for the city of Augsburg, Germany. *Urban Climate, 49*, 101472. https://doi.org/10.1016/j.uclim.2023.101472

Mokhtari, Z., Barghjelveh, S., Sayahnia, R., Karami, P., Qureshi, S., & Russo, A. (2022). Spatial pattern of the green heat sink using patch- and network-based analysis: Implication for urban temperature alleviation. *Sustainable Cities and Society, 83*, 103964. https://doi.org/10.1016/j.scs.2022.103964

Morris, C. J. G., Simmonds, I., & Plummer, N. (2001). Quantification of the Influences of Wind and Cloud on the Nocturnal Urban Heat Island of a Large City. *Journal of Applied Meteorology, 40*(2), 169–182. https://doi.org/10.1175/1520-0450(2001)040<0169:QOTIOW>2.0.CO;2

Mücke, H.-G., & Litvinovitch, J. M. (2020). Heat Extremes, Public Health Impacts, and Adaptation Policy in Germany. *International Journal of Environmental Research and Public Health, 17*(21), 7862. https://doi.org/10.3390/ijerph17217862

Neis, P., Zielstra, D., & Zipf, A. (2011). The Street Network Evolution of Crowdsourced Maps: OpenStreetMap in Germany 2007–2011. *Future Internet, 4*(1), 1–21. https://doi.org/10.3390/fi4010001

Oke, T. R. (1982). The energetic basis of the urban heat island. *Quarterly Journal of the Royal Meteorological Society, 108*(455), 1–24. https://doi.org/10.1002/qj.49710845502

Ord, J. K., & Getis, A. (1995). Local Spatial Autocorrelation Statistics: Distributional Issues and an Application. *Geographical Analysis, 27*(4), 286–306. https://doi.org/10.1111/j.1538-4632.1995.tb00912.x

Resler, J., Eben, K., Geletič, J., Krč, P., Rosecký, M., Sühring, M., … Vlček, O. (2021). Validation of the PALM model system 6.0 in a real urban environment: A case study in Dejvice, Prague, the Czech Republic. *Geoscientific Model Development, 14*(8), 4797–4842. https://doi.org/10.5194/gmd-14-4797-2021

Scherer, D., Ament, F., Emeis, S., Fehrenbach, U., Leitl, B., Scherber, K., … Vogt, U. (2019). Three-Dimensional Observation of Atmospheric Processes in Cities. *Meteorologische Zeitschrift (Berlin), 28*(2), 121–138. https://doi.org/10.1127/metz/2019/0911

Shahidan, M. F. (2015). Potential of Individual and Cluster Tree Cooling Effect Performances Through Tree Canopy Density Model Evaluation in Improving Urban Microclimate. *Current World Environment, 20*(2), 398–413. https://doi.org/10.12944/CWE.10.2.04

Siqi, J., & Yuhong, W. (2020). Effects of land use and land cover pattern on urban temperature variations: A case study in Hong Kong. *Urban Climate, 34*, 100693. https://doi.org/10.1016/j.uclim.2020.100693

Spronken-Smith, R. A., & Oke, T. R. (1998). The thermal regime of urban parks in two cities with different summer climates. *International Journal of Remote Sensing, 19*(11), 2085–2104. https://doi.org/10.1080/014311698214884

Spronken-Smith, R. A., & Oke, T. R. (1999). Scale Modelling of Nocturnal Cooling in Urban Parks. *Boundary-Layer Meteorology, 93*(2), 287–312. https://doi.org/10.1023/A:1002001408973

Stadt Augsburg (2021). Statistisches Jahrbuch der Stadt Augsburg 2020. Augsburg.

Steigerwald, F., Kossmann, M., Schau-Noppel, H., Buchholz, S., & Panferov, O. (2022). Delimitation of Urban Hot Spots and Rural Cold Air Formation Areas for Nocturnal Ventilation Studies Using Urban Climate Simulations. *Land (Basel), 11*(8), 1330. https://doi.org/10.3390/land11081330

Stewart, I. D., & Oke, T. R. (2012). Local Climate Zones for Urban Temperature Studies. *Bulletin of the American Meteorological Society, 93*(12), 1879–1900. https://doi.org/10.1175/BAMS-D-11-00019.1

Straub, A., Berger, K., Breitner, S., Cyrys, J., Geruschkat, U., Jacobeit, J., … Beck, C. (2019). Statistical modelling of spatial patterns of the urban heat island intensity in the urban environment of Augsburg, Germany. *Urban Climate, 29*, 100491. https://doi.org/10.1016/j.uclim.2019.100491

Stull, R. B. (1988). *An Introduction to Boundary Layer Meteorology*. Springer, Dordrecht. https://doi.org/10.1007/978-94-009-3027-8

Tomczyk, A. M. (2018). Hot weather in Potsdam in the years 1896–2015. *Meteorology and Atmospheric Physics, 130*(1), 1–10. https://doi.org/10.1007/s00703-016-0497-2

Unsworth, M. H., & Monteith, J. L. (1975). Long-wave radiation at the ground I. Angular distribution of incoming radiation. *Quarterly Journal of the Royal Meteorological Society, 101*(427), 13–24. https://doi.org/10.1002/qj.49710142703

Upmanis, H., Eliasson, I., & Lindqvist, S. (1998). The influence of green areas on nocturnal temperatures in a high latitude city (Göteborg, Sweden). *International Journal of Climatology, 18*(6), 681–700. https://doi.org/10.1002/(SICI)1097-0088(199805)18:6<681::AID-JOC289>3.0.CO;2-L

Vicente-Serrano, S. M., Cuadrat, J. M., & Ángel Saz-Sánchez, M. (2005). Spatial patterns of the urban heat island in Zaragoza (Spain). *Climate Research, 30*, 61–69. https://doi.org/10.3354/cr030061

Vieira Zezzo, L., Pereira Coltri, P., & Dubreuil, V. (2023). Microscale models and urban heat island studies: A systematic review. *Environmental Monitoring and Assessment, 195*(11), 1284. https://doi.org/10.1007/s10661-023-11906-2

Vogel, J., Afshari, A., Chockalingam, G., & Stadler, S. (2022). Evaluation of a novel WRF/PALM-4U coupling scheme incorporating a roughness-corrected surface layer representation. *Urban Climate, 46*, 101311. https://doi.org/10.1016/j.uclim.2022.101311

Wild, M., Behm, S., Beck, C., Cyrys, J., Schneider, A., Wolf, K., & Haupt, H. (2022). Mapping the time-varying spatial heterogeneity of temperature processes over the urban landscape of Augsburg, Germany. *Urban Climate, 43*, 101160. https://doi.org/10.1016/j.uclim.2022.101160

Wong, K. K., & Dirks, R. A. (1978). Mesoscale Perturbations on Airflow in the Urban Mixing Layer. *Journal of Applied Meteorology and Climatology, 17*(5), 677–688. https://doi.org/10.1175/1520-0450(1978)017<0677:MPOAIT>2.0.CO;2

Wouters, H., De Ridder, K., Poelmans, L., Willems, P., Brouwers, J., Hosseinzadehtalaei, P., … Demuzere, M. (2017). Heat stress increase under climate change twice as large in cities as in rural areas: A study for a densely populated midlatitude maritime region. *Geophysical Research Letters, 44*(17), 8997–9007. https://doi.org/10.1002/2017GL074889

Yan, H., Wu, F., & Dong, L. (2018). Influence of a large urban park on the local urban thermal environment. *The Science of the Total Environment, 622–623*, 882–891. https://doi.org/10.1016/j.scitotenv.2017.11.327

Yuan, C., Norford, L., & Ng, E. (2017). A semi-empirical model for the effect of trees on the urban wind environment. *Landscape and Urban Planning, 168*, 84–93. https://doi.org/10.1016/j.landurbplan.2017.09.029

Zak, M., Nita, I.-A., Dumitrescu, A., & Cheval, S. (2020). Influence of synoptic scale atmospheric circulation on the development of urban heat island in Prague and Bucharest. *Urban Climate, 34*, 100681. https://doi.org/10.1016/j.uclim.2020.100681

Manuscript received: August 13, 2024
Revisions requested: February 25, 2025
Revised version received: April 8, 2025
Manuscript accepted: April 22, 2025

The pdf version (Adobe JavaScript must be enabled) of this paper includes an electronic supplement:
Table S1; Fig. S1, S2